Evidence of field-scale shifts in transpiration dynamics following bark beetle infestation Stomatal conductance responses

Li, Meijun; Shao, Wei; Su, Ye; Coenders-Gerrits, Miriam; Jarsjö, Jerker

DOI
10.1002/hyp.15162

Publication date
2024

Document Version
Final published version

Published in
Hydrological Processes

Received: 29 May 2023 | Revised: 10 April 2024 | Accepted: 23 April 2024

DOI: 10.1002/hyp.15162

RESEARCH ARTICLE

WILEY

Evidence of field-scale shifts in transpiration dynamics following bark beetle infestation: Stomatal conductance responses

Meijun Li[1] | Wei Shao[1] | Ye Su[2,3] | Miriam Coenders-Gerrits[4] | Jerker Jarsjö[3]

[1]Key Laboratory of Hydrometeorological Disaster Mechanism and Warning, Ministry of Water Resources / School of Hydrology and Water Resources, Nanjing University of Information Science and Technology, Nanjing, China

[2]Department of Physical Geography and Geoecology, Faculty of Science, Charles University, Prague 2, Czech Republic

[3]Department of Physical Geography, and the Bolin Centre for Climate Research, Stockholm University, Stockholm, Sweden

[4]Water Resources Section, Faculty of Civil Engineering and Geosciences, Delft University of Technology, Delft, GA, The Netherlands

Correspondence
Wei Shao, Key Laboratory of Hydrometeorological Disaster Mechanism and Warning, Ministry of Water Resources / School of Hydrology and Water Resources, Nanjing University of Information Science and Technology, Nanjing, 210044, China.
Email: shao@nuist.edu.cn

Funding information
National Natural Science Foundation of China (Grant No. 41807286); Fundamental Research Project of Science and Technology Department of Qinghai Province (2023-ZJ-705); Czech Science Foundation GAČR PIF OUT project, Grant/Award Number: 242-201284

Abstract

Amplified eruptive outbreaks of bark beetles as a consequence of climate change can cause tree mortality that significantly affects terrestrial water and carbon fluxes. However, the lack of field-scale observations of underlying physiological mechanisms currently hampers the expression of such ecosystem disturbances in predictive modelling. Based on a unique flux tower dataset from a subalpine forest located in the Rocky Mountains, mechanisms of stomatal response to an extensive bark beetle outbreak were investigated using various models and parametrizations. The datasets cover a decade, including the periods of pre-infestation, infestation, and post-infestation. Field measurements showed considerable decreases in evapotranspiration (ET), transpiration (T), and leaf area index (LAI) during the two-year infestation period compared to the pre-infestation period. Model interpretations of observed water and carbon fluxes indicated that the overall reductions in T were not solely due to decreased LAI, but also to changes in physiological behaviours. The summer season's canopy-scale stomatal conductance was significantly reduced during the infestation period, from 0.0018 to 0.0011 $m\,s^{-1}$. One primary reason for the observed variations is likely that the bark beetle infestation hampers the water transport in the xylem. The damage of xylem has important implications for water use efficiency (WUE), which also significantly influences the parameterization of stomatal conductance. When using stomatal conductance models to forecast ecosystem dynamics, it is crucial to recalibrate the model's parameters to ensure the accurate depiction of stomatal dynamics during various infestation periods. The neglect of the temporal variability of canopy-scale stomatal conductance under ecosystem disturbances (e.g., bark beetle infestations) in current earth system models, therefore, requires specific attention in assessments of large-scale water and carbon balances.

KEYWORDS
bark beetle infestation, canopy-scale stomatal conductance, carbon and water fluxes, temporal variability, transpiration, vegetation-atmosphere interaction

1 | INTRODUCTION

Rising air temperatures and precipitation deficits have amplified eruptive outbreaks of bark beetles across North America, Europe, and Asia in recent decades (Goodsman et al., 2018; Hofstetter et al., 2022). The high frequency of bark beetle infestation outbreaks and the large areas of regions affected by tree mortality have significantly impacted ecohydrology (Ren et al., 2021; Seidl et al., 2017). These impacts are mainly exerted through modified canopy structures and altered physiological behaviours of infested trees (Carlson et al., 2020; Ren et al., 2023). Bark beetles can introduce a blue-stain fungus that damages the tree vascular system and interrupts the xylem flow, commonly resulting in hydraulic failure (Chen et al., 2015; Frank et al., 2019). A decrease in leaf area index (LAI) can change the energy partitioning, alter the fraction of penetrated solar radiation to the soil surface, and consequently increase sensible heat and land surface temperature of the infested area (Forzieri et al., 2020). In terms of hydrological cycling, the decreased LAI can reduce canopy transpiration and interception, while increase soil evaporation and understory transpiration (Bearup et al., 2014; Forzieri et al., 2020).

Stomatal conductance is a key parameter governing the exchange of water and CO_2 between stomata and the atmosphere (Baca Cabrera et al., 2021; Damour et al., 2010; Henry et al., 2019; Lin et al., 2015). Various stomatal conductance models have been proposed based on different conceptualizations of stomatal behaviour in response to environmental conditions (Buckley & Mott, 2013; Lamour et al., 2022; Shao et al., 2023). Jarvis et al. (1976) developed a stomatal conductance model formulated with multiple stress factors, including light density, leaf temperature, vapour pressure deficit (VPD), CO_2 concentration, and soil water potential. Several follow-up studies suggested that stomatal conductance can be a function of the photosynthesis rate at the leaf surface (Lloyd & Farquhar, 1994; Medlyn et al., 2011; Miner et al., 2017). According to this theory, Ball et al. (1987) proposed a model, in which the assimilation rate and relative humidity were positively correlated with stomatal conductance. Leuning (1995) used a similar formulation, replacing the relative humidity with the VPD. An alternative stomatal conductance model has also been formulated, based on the optimum theory that assumes that the vegetation tends to maximize the carbon gain while minimizing water consumption (Cowan & Farquhar, 1977; Lin et al., 2015; Medlyn et al., 2011). Similar model formulations were proposed by Medlyn et al. (2011) and Knauer et al. (2019). Overall, commonly-used stomatal conductance models differ widely in their mathematical formulations and underlying theories, which contributes to uncertainties in estimated transpiration (Buckley & Mott, 2013; Franks et al., 2018; Lamour et al., 2022). Therefore, the selection of an appropriate and reliable model is critical in estimating stomatal conductance and predicting transpiration.

Identifying the effects of forest disturbances on ecosystems commonly requires consistent, high-frequency monitoring of terrestrial carbon, and water fluxes, which is furthermore a prerequisite for investigating the potential variation of stomatal behaviour. The pattern of stomatal opening and closing can be affected by long-term climate change and drastic ecosystem disturbances (Buckley & Mott, 2013; Liang et al., 2023). For instance, in the long run, climate warming decreased the efficiency of water transport between stomata and the atmosphere by decreasing stomatal aperture, density, and size, which has implications for the parameterization of the stomatal conductance model (Liang et al., 2023; Lin et al., 2015). However, the main focus in parameterizing stomatal conductance models has been on the differences among vegetation species, with little consideration given to the temporal variation in the parameterization of stomatal conductance model (Bauerle et al., 2014; Damour et al., 2010; Liang et al., 2023; Xu et al., 2021).

Although the bark beetle outbreak shares similarities with other types of disturbances, such as harvest or fire, leading to dramatic removal or destruction of vegetation, it is fundamentally different in many aspects. Forest leaves and stems may be completely destroyed through combustion during fire events (Bär et al., 2019). Similarly, logging implies the removal of stems, reducing the biomass of the forest. On the contrary, after insect infestation, a certain fraction of the vegetation may survive relatively unharmed and even utilize the nutrients left by the dying trees. Moreover, bark beetle outbreaks commonly last for a relatively long period of $3 \sim 5$ years, whereas fire and logging events commonly occur over much shorter periods (Davis et al., 2020). Forests that have encountered stand-replacing fire are therefore solely composed of new vegetation replacing the dead one (Bär et al., 2019). However, in bark beetle-infested areas, the forest composition is more complex with infected trees, unharmed trees, and new trees replacing the dead ones. The infested trees and the growth of new trees may interact with each other through unknown mechanisms. Quantification of such disturbed and highly dynamic ecosystems may be difficult, especially when parameterizing the associated stomatal conductance dynamics.

This study seeks to (1) identify the influence of bark beetle infestation on the canopy-scale stomatal conductance and transpiration; (2) evaluate whether or not, and to which extent, the parameterization of stomatal conductance models needs to be altered in areas impacted by bark beetle infestation; (3) elucidate the mechanisms underlying the variation in canopy-scale stomatal conductance and transpiration under bark beetle infestation. A bark beetle-infested mature spruce forest was chosen as the study area, where the LAI, carbon flux, and water flux were observed in situ throughout periods of pre-infestation, infestation, and post-infestation. The variation in canopy-scale stomatal conductance of the spruce forest may be subject to complex mechanisms related to both a reduction of LAI and changes in physiological behaviour in response to bark beetle attacks. We parameterized stomatal conductance models (e.g., Ball-Berry model, Leuning model, and Medlyn model) separately for the three infestation periods (pre-infestation, infestation, and post-infestation), to investigate changes in the stomatal responses under the course of a bark beetle infestation event. By comparing the simulation accuracy of canopy-scale stomatal conductance and transpiration under an evolution-varied parameterization (considering all infestation stages) and a pre-infestation-fixed parameterization (considering undisturbed conditions), the impact of bark beetle infestation could be identified.

2 | DATA AND METHODS

2.1 | Study site and field instrumentation

The study is based on a high-elevation subalpine forest in the Rocky Mountains of southeastern Wyoming (41° 21.992′ N, 106° 14.397′ W, 3190 m above sea level) (Musselman, 1994). The weather features long cold winters (between −23 and −1°C). In the summer season, the air temperature ranges from −7 to 21°C. The annual average precipitation is 1200 mm/year (Speckman et al., 2015) with 70% in the form of snow (Musselman, 1994). Snow cover frequently exists from late October until July.

The land cover is mainly subalpine forest mixed with subalpine wetland and alpine tundra. Tree species are dominated by Engelmann spruce (*Picea engelmannii*) comprising 72% of the trees, while subalpine fir (*Abies lasiocarpa*) is the only companion species (Speckman et al., 2015). The canopy height is around 18 m, and LAI ranged from 4.8 to 2.8 m^2 m^{-2} from 2005 to 2014 (Frank et al., 2014).

The bark beetle infestation started in 2008, and a related severe tree disturbance developed in 2008 and 2009 (Frank et al., 2014). In 2011, it was estimated that approximately 85% of the forest basal area was infested or destroyed by bark beetles (Speckman et al., 2015). The study period can be partitioned into three infestation periods: pre-infestation (2005 ~ 2007), infestation (2008 ~ 2009), and post-infestation (2010 ~ 2014). The field monitoring was conducted at the Glacier Lakes Ecosystem Experiments Site (GLEES). The instrumentation mainly consisted of a flux tower equipped to measure meteorological forcing and water/carbon fluxes above the canopy. The 90% effective fetch of the scaffold footprint extended 0.77 ± 0.18 km (Frank et al., 2014; Gash, 1986). The study area is relatively flat with a 4% slope over 0.5 km down to a streambed before rising upward at a slope of approximately 6%. The half-hour micrometeorological forcings and carbon/water flux measurements at the GLEES Ameriflux site were described in detail by Frank et al. (2014). The data are available from the FLUXNET 2015 dataset (https://fluxnet.org/data/fluxnet2015-datase) and the GLEES Ameriflux site (https://doi.org/10.17190/AMF/1246056).

Ecosystem fluxes were measured using the eddy covariance technique. The eddy covariance sensors (model SATI/3Vx sonic anemometer, Applied Technologies, Inc., Longmont, CO and LI-7500 open-path infrared gas analyser, Li-Cor, Inc) were installed on a boom extending 2 m to the west and at 22.65 m height above the soil surface (Frank et al., 2014). Sensible heat, water vapour, and CO_2 fluxes were calculated based on the vertical wind covariance and Webb Pearman-Leuning (WPL) corrections (Gu et al., 2012; Massman & Lee, 2002; Webb et al., 1980). The terrestrial CO_2 flux was quantified as the net ecosystem production (NEP, positive representing carbon sink, and negative representing carbon source). The gross primary production (GPP) was partitioned from NEP with the night-time partitioning method (Reichstein et al., 2005). The method uses night-time temperature data to parameterize a respiration–temperature model that is then applied to the whole dataset to estimate ecosystem respiration (RECO). GPP is then calculated as the difference between RECO and NEP. Further details regarding parameterization and code can be found in Pastorello et al. (2020). The evapotranspiration (ET) was derived from latent heat measured from the eddy covariance system. The photosynthetic photon flux density (PPFD) was separated into diffuse and direct components (Campbell, 1998; Frank et al., 2014; Spitters et al., 1986). The fluxes were recorded at 20 Hz on data packer (model PAD-1202, Applied Technologies, Inc.) in serial connection to a micro-logger (CR3000, Campbell Scientific, Inc.) at a 5 min interval and resampled to 30 min. Two vertical profiles of soil temperature and volumetric water content were measured in both forest and meadow at 0.05, 0.10, 0.20, 0.51, and 1.02 m depths (Hydra probe, Vitel, Inc., Chantilly, VA), and soil heat flux was measured at 0.09 m (HFT-1, Radiation Energy Balance Systems, Inc.). Considering the possible depth measurement errors, the reported soil moisture content (SWC) in this study was weighted with measured volumetric water content at depths of 0.2, 0.5, and 1.02 m using weighting coefficients of 0.2, 0.3, and 0.5, respectively. Those measurements were also averaged over a 30-minute interval (CR10X micro-logger, Campbell Scientific, Inc.) (Frank et al., 2014).

2.2 | Penman-Monteith equation and the inverse calculation of canopy-scale stomatal conductance

Evapotranspiration ET from a vegetated area consists of transpiration T and evaporation E from the soil surface and interception. Flux tower measurements capture ET at the land surface. T was partitioned using the method proposed by Zhou et al. (2016). For this partitioning method, the relationship between T and $GPP{\cdot}VPD^{0.5}$ is assumed to be linear, suggesting that the ratio of $GPP{\cdot}VPD^{0.5}$ to T remains constant. When considering the E from the soil surface and interception, the ratio of $GPP{\cdot}VPD^{0.5}$ to ET, namely underlying water use efficiency ($uWUE = GPP{\cdot}VPD^{0.5}/T$), is expected to vary according to the faction of E (Zhou et al., 2016). If E constitutes a significant proportion of ET, the uWUE approaches zero due to the weak correlation between E and GPP. Conversely, when T dominates ET, the uWUE is high. Hence, the average uWUE can represent the ET comprised of T and average E, while the highest uWUE can reflect T. Consequently, the ratio between the highest uWUE and average uWUE can be considered equivalent to the ratio of T and ET. In this study, the 95th percentile of uWUE was chosen to denote that the T constitutes a significant portion of ET with a minimal E. The detailed theories, equations, and results for estimating transpiration rates are provided in the supplementary material.

The value of T partitioned from ET can be used to estimate canopy-scale stomatal conductance with an inverted Penman-Monteith equation (Lin et al., 2018; Monteith, 1965; Penman, 1963):

$$G_c = \frac{\gamma g_a L \rho_w T}{\Delta(R_n - L\rho_w T) + \rho_a c_p g_a (e_s - e_a) - \gamma L \rho_w T}, \quad (1)$$

where ρ_w (kg m^{-3}) is the density of water, T (m s^{-1}) is the transpiration rate, L (kJ kg^{-1}) is the latent heat of vaporization, Δ (kPa K^{-1}) is

the gradient of the saturation vapour pressure–temperature curve, R_n (W m^{-2}) represents net radiation received by vegetation canopy, e_s and e_a (kPa) are the saturated and actual vapour pressure of the air, e_s–e_a is defined as the VPD (kPa), γ (kPa K^{-1}) is the psychrometric constant, ρ_a (kg m^{-3}) and c_p (kJ kg^{-1} K^{-1}) are the density and specific heat capacity of the atmospheric air, g_a (m s^{-1}) is the aerodynamic conductance from reference a height of atmosphere (Lin et al., 2018), and G_c (m s^{-1}) is the canopy-scale stomatal conductance.

2.3 | Stomatal conductance models

2.3.1 | Ball-Berry model

In the Ball-Berry model (Ball et al., 1987), stomatal conductance $g_{s,B}$ (mol m^{-2} s^{-1}) is linked to net assimilation rate A_n (μmolCO_2 m^{-2} s^{-1}), relative humidity h_s (dimensionless), and CO_2 concentration C_s (μmolCO_2 mol^{-1}) at leaf surface, according to:

$$g_{s,B} = g_{1,B} A_n \frac{h_s}{C_s} + g_{0,B}, \quad (2)$$

where $g_{0,B}$ (mol m^{-2} s^{-1}) is the residual stomatal conductance when A_n approaches zero, $g_{1,B}$ (dimensionless) is the slope of the relationship between $A_n h_s/C_s$ (the Ball-index) and $g_{s,B}$, which is also called the stomatal sensitivity factor.

2.3.2 | Leuning model

Leuning (1995) compared two possible formulations of how stomatal conductance is related to VPD, namely a linear and a hyperbolic dependence, and proposed a hyperbolic function that may provide a more appropriate description of stomatal conductance $g_{s,L}$(mol m^{-2} s^{-1}):

$$g_{s,L} = \frac{g_{1,L} A_n}{(C_s - \Gamma)\left(1 + \frac{D}{D_0}\right)} + g_{0,L}, \quad (3)$$

where D (kPa) is the VPD at the leaf surface, Γ (μmolCO_2 mol^{-1}) is the CO_2 compensation point of photosynthesis, and $g_{0,L}$ (mol m^{-2} s^{-1}), D_0 (kPa) and $g_{1,L}$ (dimensionless) are fitted constants. Here g_0 represents the residual stomatal conductance as the A_n reaches zero, D_0 represents the sensitivity of stomatal conductance to VPD, and $g_{1,L}$ express the slope of $g_{s,L}$ and $A_n/[(C_s - \Gamma)(1 + D/D_0)]$.

2.3.3 | Medlyn model

Medlyn et al. (2011) combined optimal stomatal behaviour theory (Cowan & Farquhar, 1977) with a photosynthesis model (Farquhar et al., 1980) deriving an expression of stomatal conductance $g_{s,M}$ (mol m^{-2} s^{-1}):

$$g_{s,M} = g_{0,M} + 1.6\left(1 + \frac{g_{1,M}}{\sqrt{D}}\right)\frac{A_n}{C_s}, \quad (4)$$

where the meanings of A_n, D, and C_s are as same as the Leuning model, and the $g_{1,M}$ ($kPa^{1/2}$) is a fitted parameter representing the correlation between the $g_{s,M}$ and $A_n/\left(C_s\sqrt{D}\right)$.

2.4 | Upscaling leaf-scale stomatal conductance to canopy-scale stomatal conductance

The validity of assumptions in the Ball-Berry model (Equation 2), Leuning model (Equation 3), and Medlyn model (Equation 4) was confirmed at the leaf scale. However, in this study, stomatal conductance is estimated through an inverted Penman-Monteith equation (Equation 1) with T to represent the water exchange rate at the canopy scale. When upscaling these stomatal conductance models to the canopy scale, A_n should be approximated by gross primary production (GPP, in μmolCO_2 m^{-2} s^{-1}), representing the carbon exchange rate at the canopy scale, and D is approximated by VPD (Yu et al., 2001). Then, the leaf-level stomatal conductance (g_s) is scaled up to canopy-scale stomatal conductance (g_c).

All three models assume that g_c is positively correlated with GPP and negatively correlated with VPD, with specific relationships defined using the parameters g_0 and g_1. The parameter g_0 represents the residual stomatal conductance when GPP approaches zero, typically specified with a negligible value (De Kauwe et al., 2015). The parameter g_1 is positive to the ratio of g_c and GPP. Since g_c is positively correlated with T in the Penman-Monteith equation (Equation 1), g_1 can be considered negatively correlated with water use efficiency (WUE), reflecting vegetation physiology. A larger g_1 thus represents a smaller WUE, indicating that the vegetation tends to consume more water with the same GPP.

To estimate parameter g_1 of the stomatal conductance model, g_c is inversely estimated by the Penman-Monteith equation (Equation 1) with T. However, the unit of canopy-scale stomatal conductance in the Penman-Monteith model (G_c) is m s^{-1}. While in the stomatal conductance model, g_c uses the unit of mol m^{-2} s^{-1}. To ensure consistency of unit, the ideal gas law is used to transform the unit of G_c from m s^{-1} to mol m^{-2} s^{-1} (Pearcy & Zimmermann, 2000):

$$g_c = G_c \frac{P_a}{RT_a}, \quad (5)$$

where P_a is the atmospheric pressure (kPa), R is the dry air gas constant (0.008314 m^3 kPa K^{-1} mol^{-1}), and T_a is the air temperature (K).

2.5 | Water use efficiency

Water use efficiency (WUE, unit in g kg^{-1}) is defined as the amount of carbon gained per unit of water loss to quantify the trade-off between assimilation and transpiration (Beer et al., 2009):

$$\mathrm{WUE} = m\frac{\mathrm{GPP}}{T}, \quad (6)$$

where the unit of GPP and T is $\mu molCO_2\ m^{-2}\ s^{-1}$ and $mm\ h^{-1}$, respectively, m with the value of $1.22 \times 10^{-11}\ m^3\ \mu mol\ CO_2^{-1}$ is the constant to keep the consistency of unit. A relatively high value of WUE implies a high efficiency of photosynthesis consuming less water.

2.6 | Modelling strategies

The analysis in this study considers three periods, namely pre-infestation (2005 ~ 2007), infestation (2008 ~ 2009), and post-infestation (2010 ~ 2014), to investigate the impact of bark beetle outbreaks on the ecosystem. The variations in the daily means of observed meteorological variables (i.e., R_n, T_a, VPD) and measured water and carbon fluxes (ET and GPP) from 2005 to 2014 are presented in Section 3.1. Analysis of variance (ANOVA) was used to test for the significance of changes in observed meteorological variables (i.e., R_n, T_a, VPD) and measured water and carbon fluxes. The significance level is indicated by the p value; the smaller the value of p, the more significant the change. If $p < 0.05$, the change is considered statistically significant.

The canopy-scale stomatal conductance and transpiration were only estimated for the summer season (July and August) when the minimum air temperatures were consistently higher than 0°C. Freezing period was excluded due to negligible transpiration. The eddy covariance system provided measurement of evapotranspiration ET, which consists of transpiration T from the vegetation and evaporation E from the soil surface and interception. ET was partitioned into E and T for each year from 2005 to 2014 based on the method proposed by Zhou et al. (2016), see details in the supplementary material. T was used to estimate G_c according to the inverted Penman-Monteith equation (Equation 1). LAI was calculated based on the measurement of PAR, see the supplementary material for further detail. The results regarding LAI, partitioned T, and inversely estimated G_c in the growing season (July and August) from 2005 to 2014 are shown in Sections 3.2 and 3.3. Throughout the analysis, only values at full daylight ($R_n > 10\ W\ m^{-2}$) were used.

Three stomatal conductance models, namely Ball-Berry, Leuning, and Medlyn model were adopted to investigate the relationships between g_c and the primary drivers (i.e., GPP and VPD). Considering that g_0 is a non-sensitive parameter in a stomatal conductance model, its values were taken from the literature (De Kauwe et al., 2015; Medlyn et al., 2011). Based on the recommended parameterization sets for the Ball-Berry model and Leuning model, we used the standard parameterization of the CABLE (Community Atmosphere Biosphere Land Exchange) model ($g_0 = 0.01\ mol\ m^{-2}\ s^{-1}$, $g_1 = 9.0$, $D_0 = 1.5$ kPa for C3 vegetation) (De Kauwe et al., 2015; Oleson et al., 2013; Sellers et al., 1996). Based on the recommended parameterization of the Medlyn model, we adopted the fitted parameters of Medlyn et al. (2011) for tree species of spruce ($g_0 = 0.003\ mol\ m^{-2}\ s^{-1}$, $g_1 = 0.14\ kPa^{1/2}$). All parameterizations for the simulations are shown in the Table 1.

The g_1 parameters of three stomatal conductance models (Ball-Berry, Leuning, and Medlyn model) were calibrated using a nonlinear optimization algorithm ('lsqcurvefit' function in MATLAB software), and sampled using the Bootstrap method (Section 3.4). The Bootstrap method was used to randomly select 300 data points during the daytime (11:00 ~ 14:00) of each year's summer season, resulting in approximately 2976 data points in total. Each year, the datasets were sampled 100 times to estimate g_c using a nonlinear optimization algorithm. The probability density function (PDF) of the parameter, which was assumed to follow a Gaussian distribution, was fitted through the frequency distribution histogram (FDH) of 100 parameters.

To identify the impact of bark beetle infestation, the simulated transpiration rates using three distinct parameterization approaches within the stomatal conductance model were compared: the recommended standard parameterization for C3 vegetation, a fixed calibration parameterization (referred to as pre-infestation-fixed parameterization) that refers to undisturbed conditions prior to infestation without accounting for subsequent disturbances, and an adaptive parameterization (named evolution-varied parameterization) that was calibrated annually from 2005 to 2014 to incorporate the effects of all three stages of disturbance. In Sections 3.5 and 3.6, the pre-infestation-fixed parameterization was fitted using daytime data of July and August during the pre-infestation period (2005 ~ 2007) to represent the physiological behaviour of undisturbed trees. The evolution-varied parameterization was fitted each year from 2005 to 2014 using the daytime data of July and August to reflect physiological behaviours under bark beetle infestation. Both the pre-infestation-fixed parameterization and the evolution-varied parameterization were used in stomatal conductance models (Section 2.3) and the Penman-Monteith equation (Equation 1) to estimate g_c and T. Then the impacts of bark beetle infestation on g_c and T were revealed by comparing differences between the pre-infestation-fixed parameterization and the evolution-varied parameterization.

3 | RESULTS

3.1 | Variation in meteorological variables, carbon and water fluxes

The daily means of the measured meteorological variables (R_n, T_a, and VPD) and water and carbon fluxes (ET and GPP) in the GLEES station in southwestern Wyoming from 2005 and 2014 are shown in Figure 1. The meteorological forcing variables showed a strong seasonal variation but negligible annual or inter-annual variability. The daily means of R_n ranged between 5 and 250 $W\ m^{-2}$, reflecting seasonal variations, but its inter-annual variability or trend across different infestation periods was not significant ($p = 0.0169$; Figure 1a). The T_a values fluctuated between −20 and 17°C in close correlation with R_n (Figure 1b). The daily mean VPD values commonly ranged between 0 and 1.5 kPa without a significant inter-annual trend across different infestation periods ($p = 0.4939$; Figure 1c).

The bark beetle outbreak significantly reduced GPP ($p < 0.0001$) and ET ($p < 0.0001$) since 2008 (Figure 1d). The annual mean GPP decreased from 2.03 $\mu molCO_2\ m^{-2}\ s^{-1}$ in the pre-infestation period

TABLE 1 The parameters of the three stomatal conductance models (Ball-Berry, Leuning and Medlyn model) are given including recommended parameterization from published literatures (De Kauwe et al., 2015; Medlyn et al., 2011), the pre-infestation-fixed fitting parameterization, and the evolution-varied parameterization.

		Ball-Berry		Leuning		Medlyn	
		$g_{0,B}$ (mol m^{-2} s^{-1})	$g_{1,B}$ (–)	$g_{0,L}$ (mol m^{-2} s^{-1})	$g_{1,L}$ (–)	$g_{0,M}$ (mol m^{-2} s^{-1})	$g_{1,M}$ (kPa$^{1/2}$)
Recommended		0.01	9.00	0.01	9	0.003	0.14
Pre-infestation-fixed		0.01	2.12	0.01	1.48	0.003	−0.26
Evolution-varied	2005	0.01	2.40	0.01	1.65	0.003	−0.16
	2006	0.01	2.23	0.01	1.57	0.003	−0.22
	2007	0.01	1.79	0.01	1.30	0.003	−0.33
	2008	0.01	1.79	0.01	1.14	0.003	−0.40
	2009	0.01	1.84	0.01	1.18	0.003	−0.30
	2010	0.01	2.05	0.01	1.52	0.003	−0.13
	2011	0.01	1.89	0.01	1.22	0.003	−0.31
	2012	0.01	1.32	0.01	0.89	0.003	−0.48
	2013	0.01	1.35	0.01	0.95	0.003	−0.43
	2014	0.01	1.24	0.01	0.89	0.003	−0.35

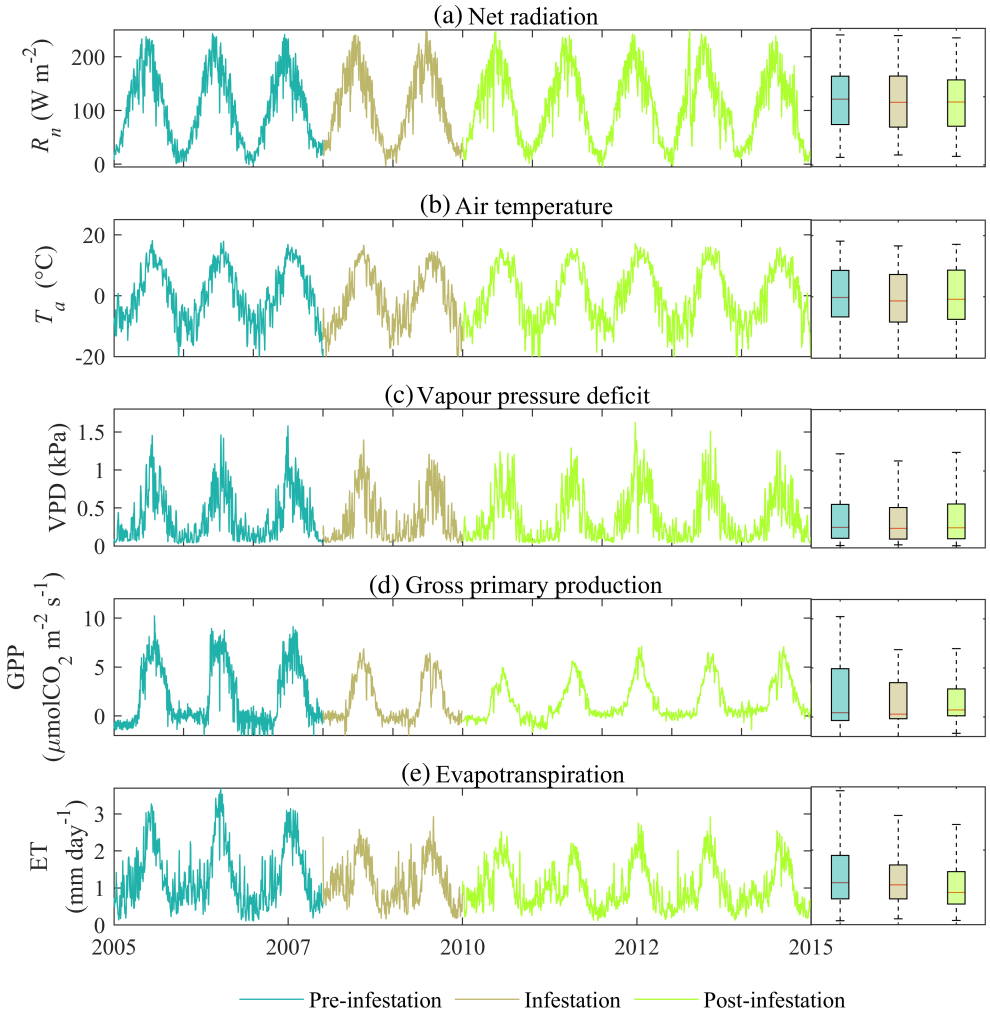

FIGURE 1 The daily mean of meteorological forcing variables and carbon and water flux ((a) net radiation R_n; (b) air temperature T_a; (c) vapour pressure deficit VPD; (d) gross primary production GPP; (e) evapotranspiration ET) from 2005 to 2014.

to 1.45 μmol CO_2 m^{-2} s^{-1} in the post-infestation period. During the post-infestation period, daily mean GPP values showed an increasing trend, but the increase was not statistically significant ($p = 0.508$), which was consistent with the ongoing recovery of the forest ecosystem. The daily mean ET values were between 0.11 and 3.69 mm day^{-1} depending on season. The peak values of daily mean

ET decreased significantly from 3.15 mm day^{-1} in 2007 to less than 2.58 mm day^{-1} in 2008 (Figure 1e). During the post-infestation period, the peak values of daily mean ET recovered significantly ($p < 0.0001$) but still did not reach the same magnitude as those in the pre-infestation period.

3.2 | Partitioning of evapotranspiration

Under typical conditions, the bark beetle infestation leads to a reduction in LAI, consequently influencing the *T*/ET ratio. Figure 2 shows box plots representing ET, the *T*/ET ratio, and partitioned *T* and *E* during three distinct infestation periods: pre-infestation, infestation, and post-infestation.

The median value of ET decreased from 2.43 mm day^{-1} in the pre-infestation period to 2.19 mm day^{-1} in the infestation period ($p < 0.0001$). The *T*/ET ratio decreased from 0.46 in the pre-infestation period to 0.43 in the infestation period indicating a significant decrease in *T* ($p < 0.0001$). The decreases in ET can mainly be attributed to the decrease in *T*. The transition from the pre-infestation period to the infestation period was accompanied by the decrease of *T* from 1.14 to 0.94 mm day^{-1} ($p < 0.0001$), whereas *E* decreased slightly from 1.27 to 1.25 mm day^{-1} ($p < 0.0001$).

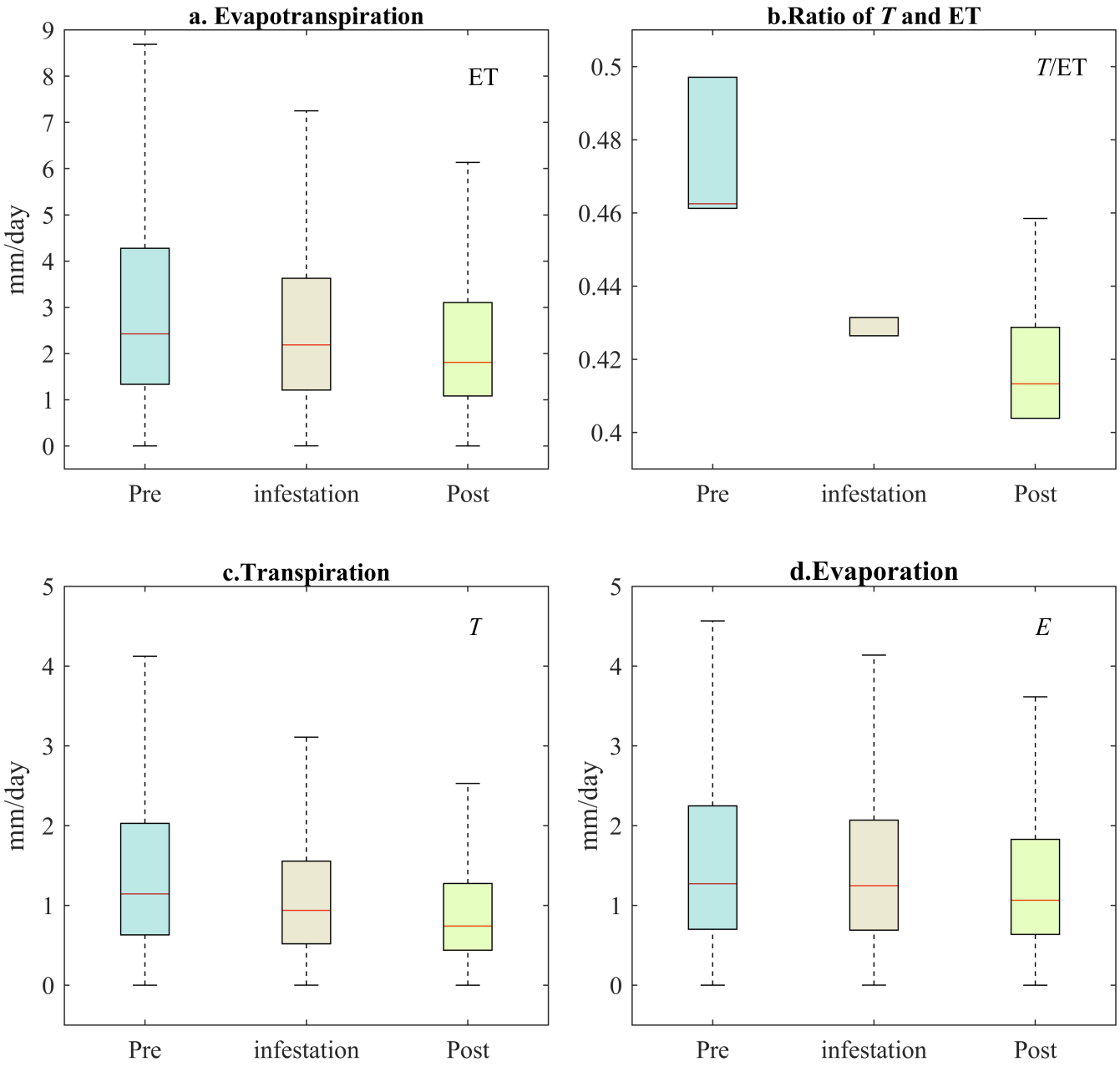

FIGURE 2 Box plots of evapotranspiration ET, *T*/ET, transpiration *T*, and soil evaporation *E* in pre-infestation periods (bule box), infestation periods (grey box), and post-infestation periods (green box).

During the post-infestation period, the values of ET, *T*, and *E* continued to decrease. The median values of ET decreased from 2.19 mm day^{-1} in the infestation period to 1.81 mm day^{-1} in the post-infestation period ($p < 0.0001$). The median value of *T* decreased from 0.94 mm day^{-1} in the infestation period to 0.74 mm day^{-1} in the post-infestation period ($p < 0.0001$). The median value of *E* decreased from 1.25 mm day^{-1} in the infestation period to 1.06 mm day^{-1} in the post-infestation period ($p < 0.0001$).

3.3 | Variations in LAI, transpiration, and canopy-scale stomatal conductance

The box plots of annual LAI, *T*, and G_c from 2005 to 2014 are shown in Figure 3. In the pre-infestation period, the LAI fluctuated around 4.51 m^2 m^{-2}. As the infested trees died from 2008 to 2011, the LAI decreased from 4.55 m^2 m^{-2} in 2007 to 2.92 m^2 m^{-2} in 2011 ($p < 0.0001$). In the post-infestation period, the LAI tended to be stable with an annual mean value of 3.06 m^2 m^{-2} (Figure 3a).

In the pre-infestation period, the *T* and G_c fluctuated around 2.15 mm day^{-1} and 1.8 × 10^{-3} m s^{-1}. After the onset of the bark beetle infestation period in 2008, the *T* and G_c significantly decreased ($p < 0.0001$). The annual mean of *T* decreased from 2.09 mm day^{-1} in 2007 to 1.57 mm day^{-1} in 2008 (Figure 3b). The annual mean G_c decreased significantly from 1.6 × 10^{-3} m s^{-1} in 2007 to less than 1.1 × 10^{-3} m s^{-1} in 2008 (Figure 3c). After 2008, the annual mean value of *T* and G_c fluctuated within small ranges, from 1.51 mm day^{-1} to 1.2 m day^{-1} and from 9.7 × 10^{-4} to 1.0 × 10^{-3} m s^{-1}, respectively.

Reductions in LAI should, in theory, be accompanied by decreases in both *T* and G_c, that is, in the absence of other influencing factors. The current results showed a significant decrease in LAI during the period 2009 ~ 2011 ($p < 0.0001$). However, the variations in

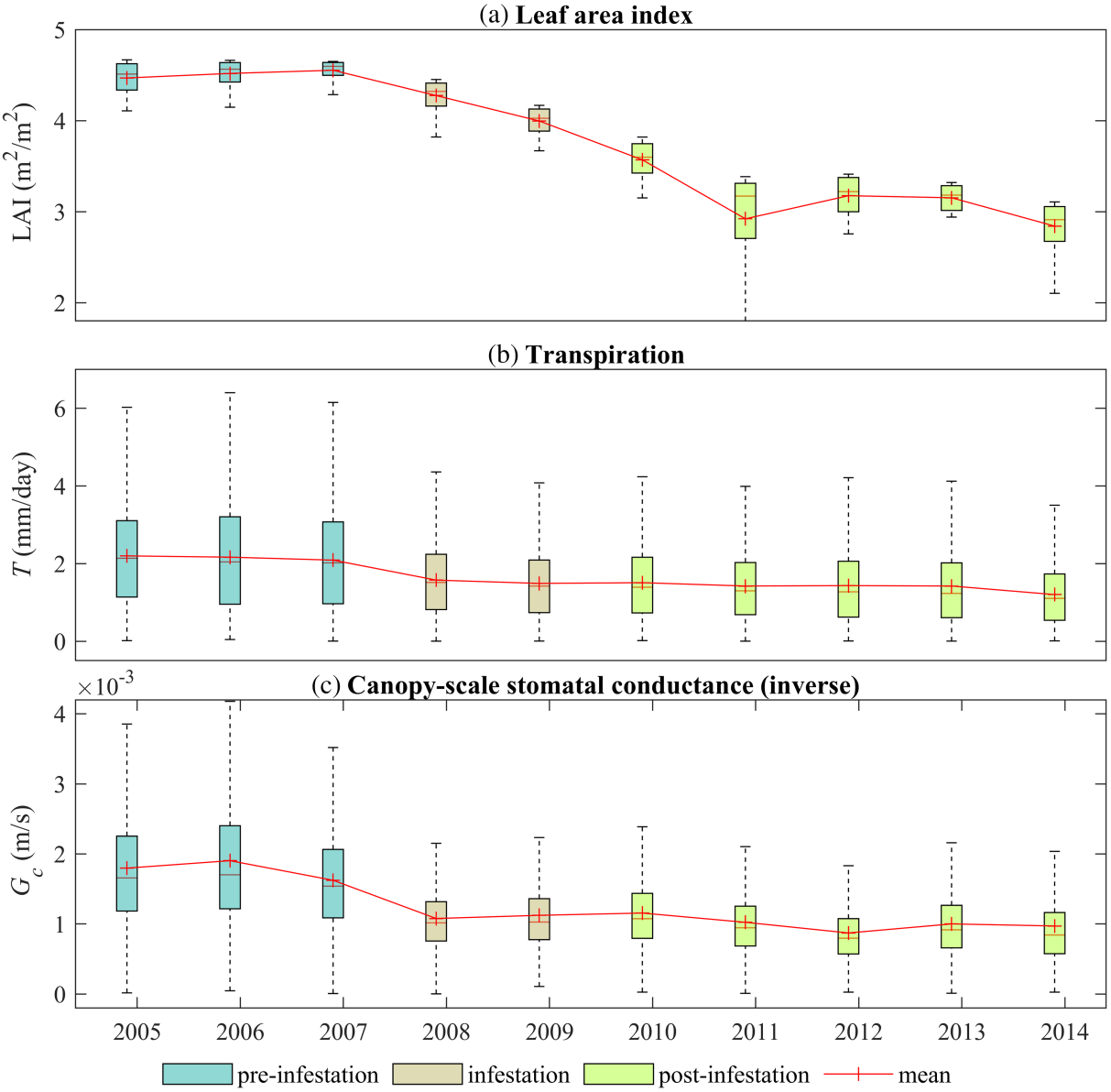

FIGURE 3 Box plots of (a) leaf area index LAI, (b) transpiration *T*, and (c) canopy-scale stomatal conductance G_c in July and August from 2005 to 2014.

T ($p = 0.1526$) and G_c ($p = 0.6131$) did not exhibit a significant decrease comparable to LAI. The distinct patterns observed in the changes between LAI and the patterns of T and G_c may therefore be attributed to other factors, such as the variation in the physiological characteristics of insect-affected trees, as discussed in detail in Section 4.

3.4 | Fitted parameter g_1 for three stomatal conductance models and three infestation periods

The parameter g_1 represents the correlation between g_c and GPP in the stomatal conductance models. Considering the positive correlation between g_c and T in the Penman-Monteith equation (Equation 1), g_1 is consequently negatively correlated with water use efficiency (WUE), reflecting vegetation physiology. The physiological characteristics of plants are therefore represented by the probability distributions of g_1. Employing the Bootstrap method as described in Section 2.6, the probability distribution function (PDF) of parameter g_1 for each year was constructed by fitting frequency distribution histograms of 100 parameters. The PDFs of parameter g_1 in the Ball-Berry, Leuning, and Medlyn models are shown as violin plots in Figure 4.

The value ranges of parameter g_1 differed among the stomatal conductance models. In the Ball-Berry model, the values of g_1 varied from 3.39 to 8.86. The fitted g_1 values were lower in the Leuning

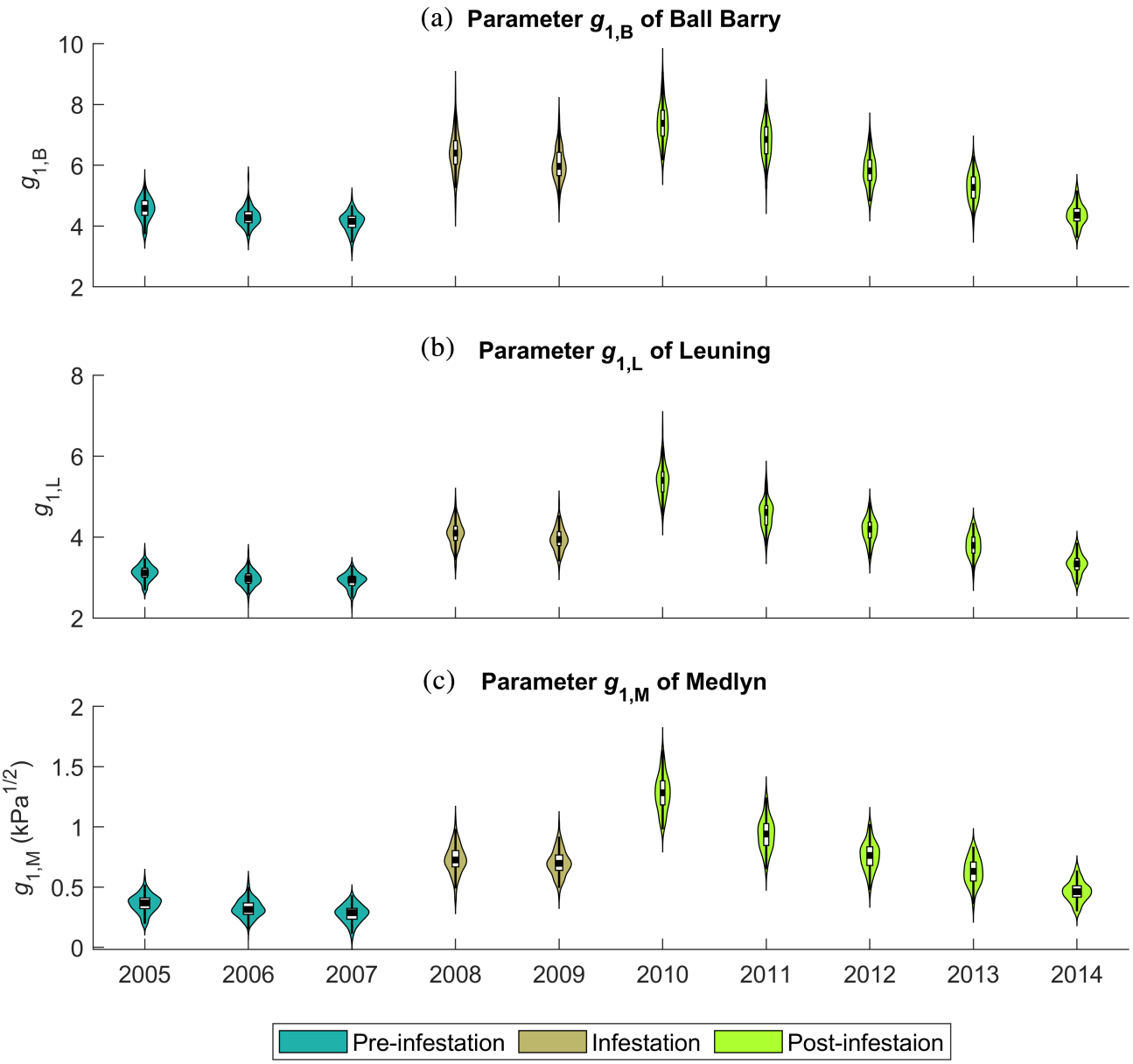

FIGURE 4 The probability distribution for the parameters of g_1 fitted from 2005 to 2014 of the three stomatal conductance models ((a) Ball-Berry, (b) Leuning, and (c) Medlyn model).

model, ranging from 2.43 to 6.50, as the Leuning model took the CO_2 compensation point (Γ) of photosynthesis into account. The parameter g_1 in the Medlyn model considered the influence of a higher diffusion rate (=1.6) of water vapour than CO_2. The estimated value of g_1 in the Medlyn model ranged from 0.077 to 1.63.

The fitted parameter values of g_1 in the three stomatal conductance models showed consistent trends of drastic increases in the infestation period and gradual decreases due to the recovery in the post-infestation period (Figure 4). In 2010, the values of parameter g_1 showed a significant increase. The consistent trends of the g_1 values in different models provided robust evidence of changes in the vegetation physiology due to the bark beetle infestation.

3.5 | Simulated G_c and T using recommended parametrization, and calibrated parametrization with pre-infestation-fixed or evolution-varied periods

The accuracy of simulated G_c and T under three parameterizations (recommended, pre-infestation-fixed, and evolution-varied) of the Ball-Berry, Leuning, and Medlyn models is evaluated using standard deviation (SD), correlation coefficient, and root mean square deviation (RMSD) as shown in the Taylor diagram in Figure 5. The average SD and RMSD of G_c using the recommended parameterization were 2.24×10^{-3} and 1.67×10^{-3} m s^{-1}, respectively. The high values of SD and RMSD of simulated G_c indicated large margins of errors when employing the recommended standard parametrization to represent the physiological behaviours of subalpine forests located in the Rocky Mountains (De Kauwe et al., 2015; Medlyn et al., 2011). The fitted G_c exhibited smaller errors compared to the recommended standard parametrization. The average SD and RMSD of G_c using pre-infestation-fixed parameterization were 5.05×10^{-4} and 7.36×10^{-4} m s^{-1}, respectively. Further reductions in errors in simulated G_c were achieved with the evolution-varied parameterization, resulting in a smaller SD of 5.00×10^{-4} m s^{-1} and smaller RMSD of 7.09×10^{-4} m s^{-1}.

Errors in the recommended standard parameterization of G_c can propagate to estimated transpiration. Employing the recommended parameterization of G_c led to relatively large errors in simulated T, with an average SD of 0.214 mm h^{-1} and an average RMSD of 0.167 mm h^{-1}. The improved G_c-values from the evolution-varied parameterization reduced the simulated error of T (SD and RMSD of 0.0859 and 0.0466 mm h^{-1}), also compared to the pre-infestation-fixed parameterization (SD and RMSD of 0.0878 and 0.0488 mm h^{-1}).

3.6 | The diurnal variation of G_c and T during three infestation periods, based on flux tower data and variously parametrized stomatal conductance models

Figure 6 shows the diurnal variation of the inversely estimated G_c (from flux tower data and the Penman-Monteith's equation), compared to simulated G_c using recommended-standard parametrization, and calibrated parametrization (pre-infestation-fixed and evolution-varied), based on the three models of Ball-Berry, Leuning, and Medlyn. The corresponding diurnal variations of simulated and measured T are shown in Figure 7. The average errors of the simulated G_c and T (equal to the difference between simulation and observation) in three infestation periods are shown in Table 2.

Throughout the three infestation periods, the recommended standard parameterization overestimated G_c. Compared with the inverse modelling of the flux tower data in the pre-infestation period, the stomatal conductance models of both Ball-Berry and Leuning

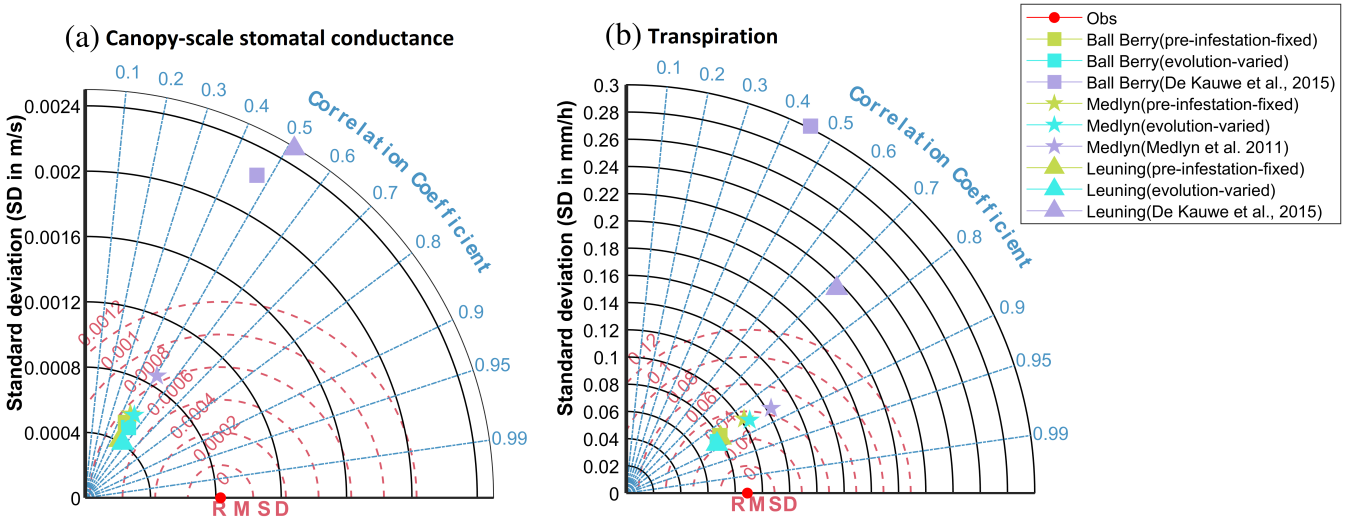

FIGURE 5 The standard deviation (SD), root mean square deviation (RMSD) and correlation coefficient of G_c and T simulated by the Ball-Berry, Leuning, and Medlyn stomatal conductance model with recommended parameterization, pre-infestation-fixed parameterization, and annual evolution-varied parameterization respectively.

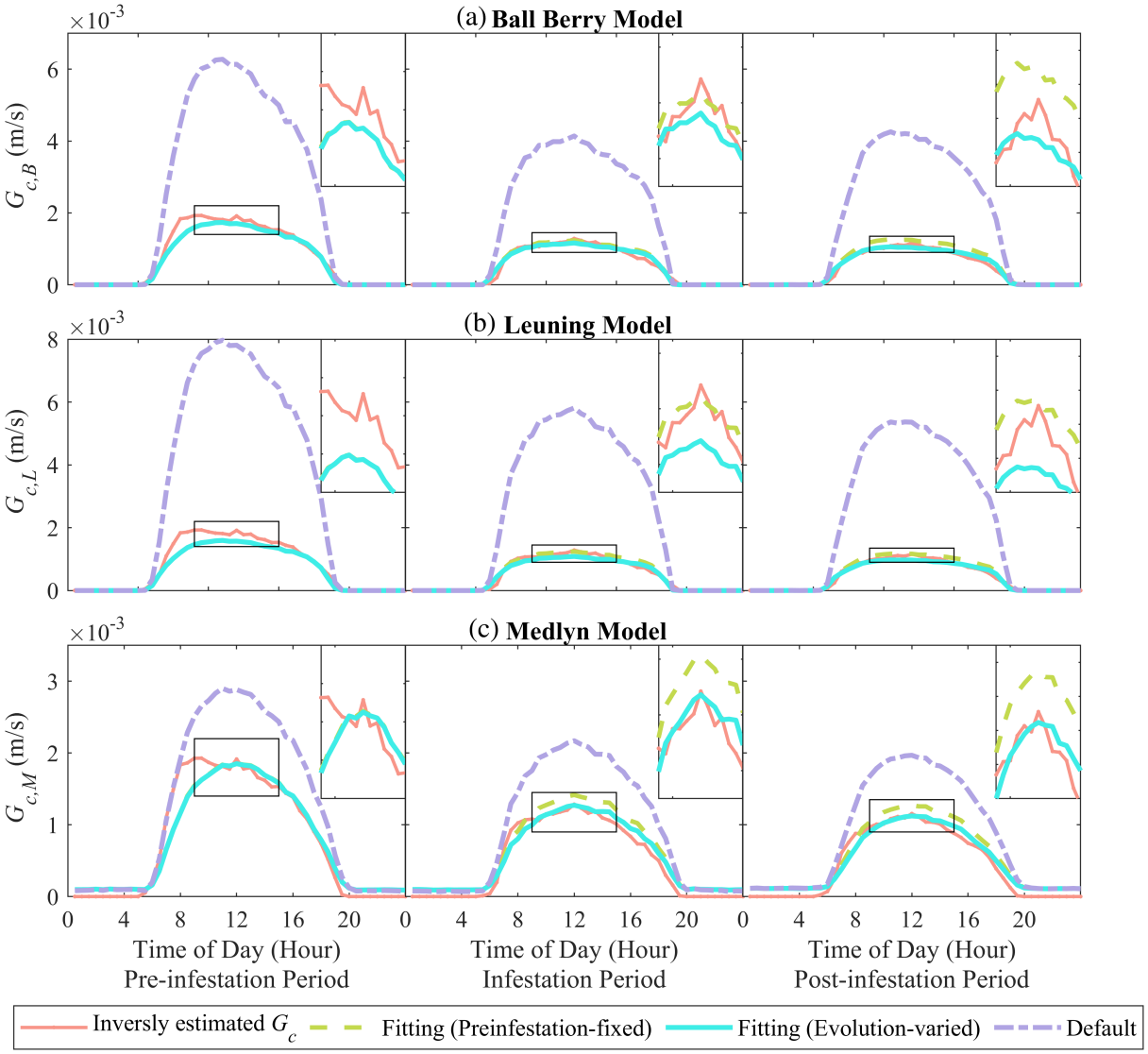

FIGURE 6 The average diurnal variation in G_c from inverse modelling of flux tower data (red line), compared to stomatal conductance modelling with recommended standard parametrization (purple dotted line), and pre-infestation-fixed parameterization (blue line) and annual evolution-varied parameterization (green line), using (a) Ball-Berry, (b) Leuning, and (c) Medlyn models. The small inset at the upper right depicts an amplified image within a black frame, showcasing the diurnal peak value of G_c.

underestimated G_c. The Medlyn model can describe the G_c more accurately. The parameterization of G_c can significantly affect simulated T. The Medlyn model provided a more accurate description of G_c compared with the other two models (Figure 6c), which finally brought the best-fitted simulation of T (Figure 7c).

The stomatal conductance models using pre-infestation-fixed parameterization overestimated G_c, especially in the post-infestation period. In comparison, the evolution-varied parameterization effectively reduced the average error of G_c. The average errors of G_c using the pre-infestation-fixed parameterization were 6.24×10^{-5} m s^{-1} (12.7% of the daily mean G_c) in the infestation period, and 8.89×10^{-5} m s^{-1} (20.2% of the daily mean G_c) in the post-infestation period. The simulated errors of G_c using the evolution-varied parameterization were 1.23×10^{-5} m s^{-1} (2.56% of the daily mean G_c) in the infestation period, and 1.57×10^{-5} m s^{-1} (3.56% of the daily mean G_c) in the post-infestation period.

Similar to G_c, the pre-infestation-fixed parameterization led to an overestimation of T after the outbreak of the bark beetle. However, the evolution-varied parameterization can reduce the simulated error of T. The average errors of simulated T using the evolution-varied parameterization were 6.32×10^{-4} mm h^{-1} (1.16% of the daily mean T) during the infestation period and 6.44×10^{-4} mm h^{-1} (1.32% of the daily mean T) during the post-infestation period. In contrast, employing the pre-infestation-fixed parameterization led to the overestimation of T by 48.2×10^{-4} mm h^{-1} (8.82% of the daily mean T)

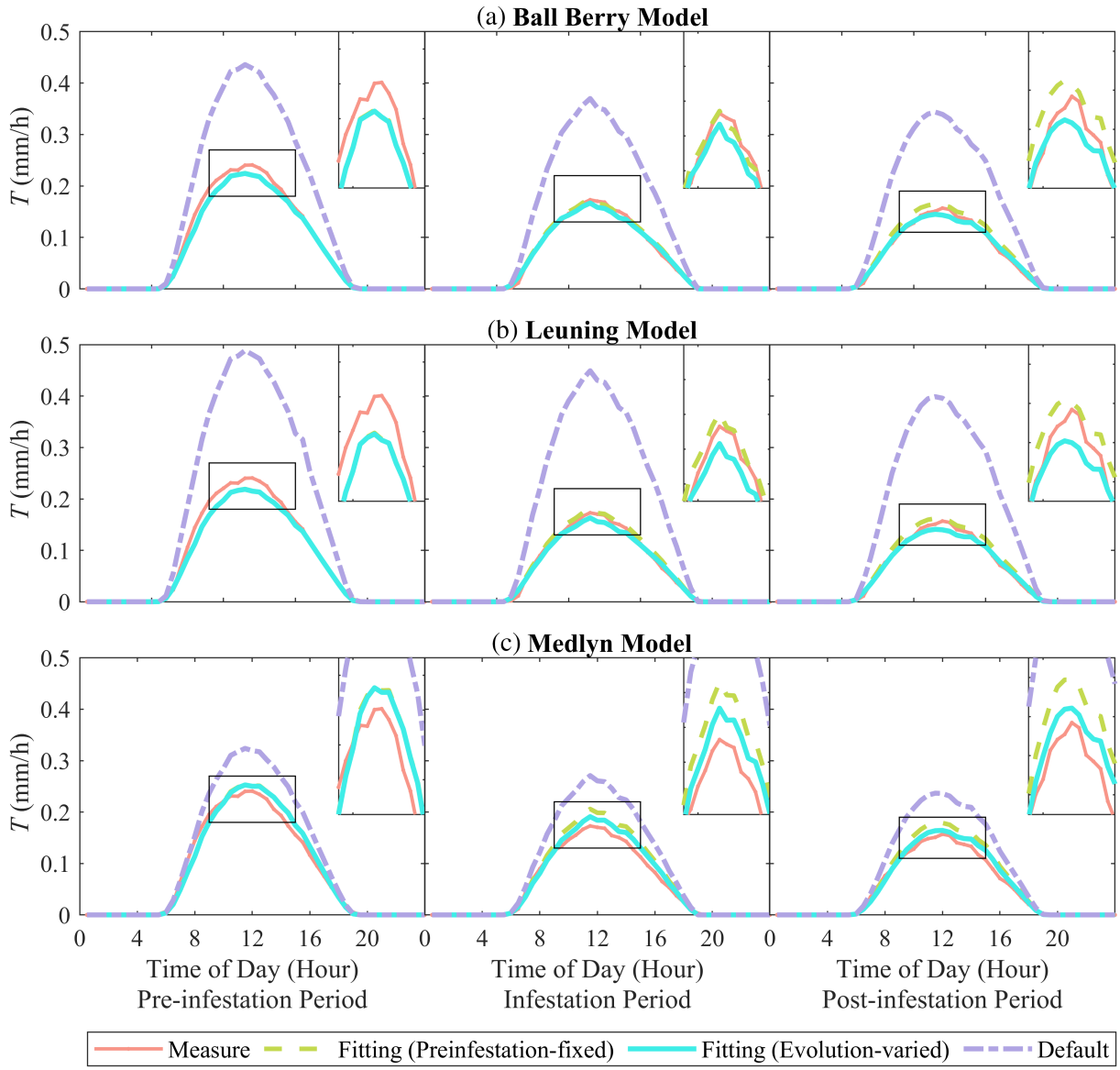

FIGURE 7 The average diurnal variation in measured *T* (red line), compared to estimated *T* using stomatal conductance modelling with recommended standard parameterization (purple dotted line), pre-infestation-fixed parameterization (blue line) and annual evolution-varied parameterization (green line), using (a) Ball-Berry, (b) Leuning, and (c) Medlyn models. The small inset at the upper right depicts an amplified image within a black frame, showcasing the diurnal peak value of *T*.

TABLE 2 The average error of the simulated G_c and *T* (equal to the difference between simulated value and measured value) with pre-infestation-fixed parameterization and evolution-varied parameterization across three different infestation periods: pre-infestation, infestation, and post-infestation period.

		Ball-Berry		Leuning		Medlyn	
		Pre-infestation-fixed	Evolution-varied	Pre-infestation-fixed	Evolution-varied	Pre-infestation-fixed	Evolution-varied
G_c (m s^{-1})	Pre	-7.76×10^{-5}	-7.85×10^{-5}	12.8×10^{-5}	12.8×10^{-5}	0.460×10^{-5}	0.674×10^{-5}
	Infestation	3.19×10^{-5}	0.346×10^{-5}	3.33×10^{-5}	-2.83×10^{-5}	12.2×10^{-5}	6.25×10^{-5}
	Post	9.22×10^{-5}	1.04×10^{-5}	5.77×10^{-5}	-1.96×10^{-5}	11.7×10^{-5}	5.62×10^{-5}
T (mm h^{-1})	Pre	-5.43×10^{-3}	-5.58×10^{-3}	-6.89×10^{-3}	-7.03×10^{-3}	2.19×10^{-3}	1.83×10^{-3}
	Infestation	1.52×10^{-3}	0.822×10^{-3}	3.48×10^{-3}	-1.96×10^{-3}	9.45×10^{-3}	4.68×10^{-3}
	Post	6.25×10^{-3}	-0.106×10^{-3}	5.22×10^{-3}	-1.44×10^{-3}	3.49×10^{-3}	8.54×10^{-3}

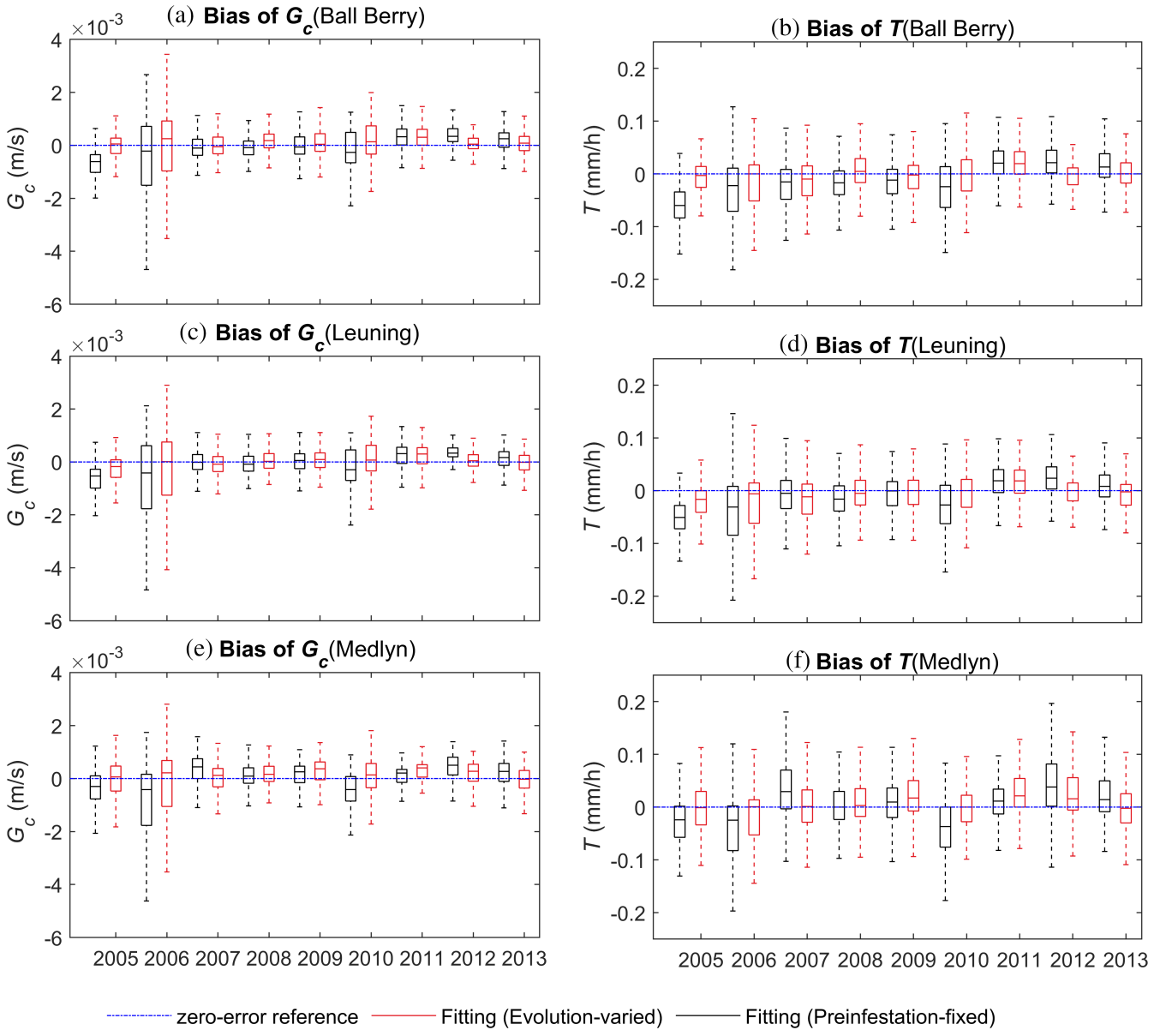

FIGURE 8 Box plots of bias of simulated G_c and T in comparison with pre-infestation-fixed parametrization and annual evolution-varied parametrization based on the Ball-Berry, Leuning, and Medlyn models.

during the infestation period and by 66.7 × 10^{-4} mm h^{-1} (13.6% of the daily mean T) during the post-infestation period.

3.7 | Bias of simulated G_c and T using pre-infestation-fixed parameterization and evolution-varied parameterization

Box plots illustrating the biases, defined as the difference between simulation and observation, of G_c and T based on the pre-infestation-fixed parameterization and the evolution-varied parameterization of the Ball-Berry, Leuning, and Medlyn models are presented in Figure 8. Overall, performance utilizing the evolution-varied parameterization was notably superior to those employing the pre-infestation-fixed parameterization. Across the entire study period (2005 ~ 2014), the average biases of G_c and T using the pre-infestation-fixed parameterization were − 17.5 × 10^{-5} m s^{-1} and − 16.8 × 10^{-3} mm h^{-1}, whereas evolution-varied parameterization led to much smaller biases of − 5.35 × 10^{-5} m s^{-1} and − 8.69 × 10^{-3} mm h^{-1}.

The average biases of G_c and T using the evolution-varied parameterization were 2.79 × 10^{-5} m s^{-1} and 4.26 × 10^{-3} mm h^{-1} in the Medlyn model, which were the smallest among the three stomatal conductance models. For the Ball-Berry model, the average biases of G_c and T were − 2.96 × 10^{-5} m s^{-1} and 11.1 × 10^{-3} mm h^{-1}, respectively, while for the Leuning model,

they were -15.9×10^{-5} m s^{-1} and -19.2×10^{-3} mm h^{-1}. During the post-infestation period from 2011 to 2014, the average biases of G_c and T shifted from negative to positive when using the pre-infestation-fixed parameterization, indicating a significant overestimation of G_c and T values by the pre-infestation-fixed parameterization.

4 | DISCUSSION

4.1 | Dominant factors of water flux in the bark beetle infestation region

Evapotranspiration (ET) plays a pivotal role in regulating both surface water and groundwater recharge, holding critical significance for water resources (Ren et al., 2021; Yang et al., 2020). Ecological disturbances, such as those induced by bark beetle activity, can change the hydrological partitioning between evaporation (E) and transpiration (T) (Schreiner-McGraw et al., 2022). Previous analysis of hydrological impacts related to bark beetle-induced forest mortality have suggested that bark beetle infestation can reduce ET and lead to an increase in streamflow (Frank et al., 2014; Vystavna et al., 2018; Wehner & Stednick, 2017). In this study, the bark beetle has been observed causing a substantial decrease in ET and T, as illustrated in Figures 2 and 3.

As expressed by the Penman-Monteith equation, T is known to be sensitive to meteorological variables, particularly R_n, T_a, e_a, and U, as well as soil water content (SWC) and vegetation characteristics (e.g. G_c). The ranges of SWC during the three infestation periods are shown in Figure 9. SWC increased throughout the infestation period, suggesting that the decreases in T were not limited by water stress and related SWC deficiency.

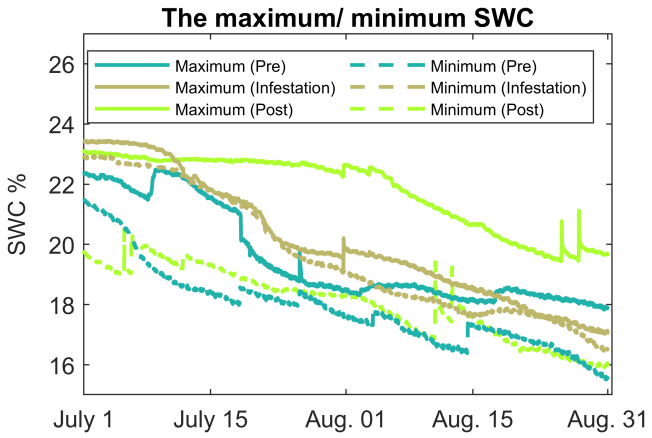

FIGURE 9 Range of soil water content (SWC) throughout July and August across three distinct periods: pre-infestation, infestation, and post-infestation. The blue, brown, and green lines represent the SWC observed in pre-infestation, infestation, and post-infestation, respectively. The solid line was the maximum SWC, while the dotted line was the minimum SWC.

Additionally, a previous study indicated that the study area was not strongly water-limited, resulting in minimal impacts on transpiration and stomatal conductance (Frank et al., 2014). Therefore, this study focuses on meteorological factors and canopy-scale stomatal conductance to identify the key factors influencing the decrease in T.

The contribution of meteorological factors and stomatal conductance to the decrease in T during the bark beetle infestation is evaluated, considering the method proposed by Zheng et al. (2009), by estimating the sensitivity of T to the other variables (R_n, T_a, e_a, U, and G_c) multiplied by the average annual-variation rate of each variable (d/dt). All the variables were normalized. The sensitivities of T to the other variables are estimated through multilinear regression, expressing the partial derivative of T with respect to each variable ($\partial T/\partial$) during the study period (2005 $\sim$ 2014) (Zheng et al., 2009), as shown in Table 3.

The analysis shows that G_c predominantly contributes to the reduction of T, whereas the impact of meteorological factors (U, R_n, T_a, e_a) on T is relatively minor. The contribution of U to the decrease in T was the smallest. Although T_a and e_a among the meteorological factors were sensitive to T, their influences remained significantly less pronounced compared to G_c. Consequently, climate variability can be dismissed as the primary underlying mechanism for the reduction in T over the outbreak. The primary cause for the decline in T is attributed to factors related to vegetation characteristics, with G_c identified as the key contributor. Thus, accurate parameterization of G_c is crucial for precise transpiration estimates and simulation of ecosystem hydrological processes, particularly during infestation periods.

The value of G_c depends on both the vegetation coverage and the vegetation physiology. The vegetation coverage can be represented by LAI, while the vegetation physiology is reflected by the PDF of the parameter g_1 (see Section 3.4), which in turn is related to WUE. The method proposed by Zheng et al. (2009) was used to determine the contributions of LAI and vegetation physiology (g_1) to G_c under bark beetle infestation. Parameters $g_{1,B}$, $g_{1,L}$, and $g_{1,M}$ from three stomatal conductance models were analysed. The results are presented in Table 4. Throughout the infestation period, the reductions in G_c were predominantly attributed to a decrease in LAI, with g_1 also exerting a significant impact. An increase in the g_1 parameter during the infestation period can mitigate 16.7% to 57.1% of the decrease in G_c caused by the decline in LAI. However, during both the pre-infestation and post-infestation periods, g_1 was the primary influencing factor on G_c.

4.2 | Correlation of LAI and canopy-scale stomatal conductance in bark beetle infestation

Generally, G_c is expected to be positively correlated with LAI (e.g., in the Jarvis model, the G_c is equal to the multiplication of LAI and stress functions (Jarvis et al., 1976)). However, bark beetle infestation may alter the relationship between LAI and G_c. To delve deeper into this

TABLE 3 The annual gradient of net radiation (R_n), air temperature (T_a), vapour pressure (e_a), wind speed (U), and canopy-scale stomatal conductance (G_c), and the contribution of these environmental factors on transpiration (T) from 2005 to 2014.

Variable (x)	R_n	T_a	e_a	U	G_c
T contribution	−0.0271	−0.0324	−0.0797	0.0071	1.1320
$\partial T/\partial x$	−0.0792	0.1455	0.0972	−0.0390	1.1054
dx/dt	−0.0319	0.0207	0.0765	0.0171	−0.0955

Note: x represents a variable of influencing factor (e.g., R_n, T_a, e_a, U, and G_c); $\partial T/\partial x$ is the correlation coefficient between T influencing factor x; dx/dt is the temporal trend of influencing factor x.

TABLE 4 The annual gradient of LAI, and g_1, and the contribution of these environmental factors on canopy-scale stomatal conductance (G_c) during pre-infestation, infestation, and post-infestation period.

		Ball-Berry		Leuning		Medlyn	
	Variable (x)	LAI	$g_{1,B}$	LAI	$g_{1,L}$	LAI	$g_{1,M}$
Pre-infestation	G_c contribution	−0.0153	1.0153	−0.0494	1.0494	−0.0313	1.0313
	$\partial G_c/\partial x$	0.0402	1.0153	−0.0494	1.0494	−0.0313	1.0313
	dx/dt	0.1902	−0.5000	0.1902	−0.5000	0.1902	−0.5000
Infestation	G_c contribution	1.2012	−0.2012	1.5685	−0.5685	2.3289	−1.3289
	$\partial G_c/\partial x$	0.9797	−0.2012	1.5685	−0.5685	2.3289	−1.3289
	dx/dt	−0.3415	0.3154	−0.3415	0.2377	−0.3415	0.3016
Post-infestation	G_c contribution	−0.3379	1.3379	−0.7246	1.7246	−0.1033	1.1033
	$\partial G_c/\partial x$	−0.3376	1.3379	−0.7246	1.7246	−0.1033	1.1033
	dx/dt	−0.1871	−0.2734	−0.1871	−0.2402	−0.1871	−0.1540

Note: x represents a variable of influencing factor (e.g. LAI and g_1); $\partial G_c/\partial x$ is the correlation coefficient between G_c and influencing factor x; dx/dt is the long-term trend of influencing factor x.

phenomenon, departing from the current dataset characterized by relatively high R_n and SWC, we performed a linear regression analysis between LAI and G_c. This involves sorting the data from each infestation period in descending order and selecting the largest 30% of R_n and SWC. The probability distributions of G_c and LAI is approximated to Gaussian distributions to elucidate their variations across different infestation periods.

The correlations between G_c and LAI showed notable variability after the bark beetle infestation occurred (Figure 10). The positive slope in G_c and LAI during the pre-infestation period changed to a negative correlation during the infestation period. Subsequently, it rebounded to a positive correlation in the post-infestation period, providing clear evidence of discernible changes in the physiological behaviour of the vegetation as bark beetles impacted the trees in the region.

Studies indicated that a large number of needle leaves dropped 1 to 2 year after the trees had been infested (Frank et al., 2014; Hubbard et al., 2001; Reed et al., 2018). Frank et al. (2014) suggested that bark beetles reduce the water flow from the root and canopy by supporting the development of blue-stain fungi during and after infestation, potentially explaining alterations the in LAI and G_c. Hydraulic failure in trees shortly after infestation with blue fungi results in a rapid decrease in G_c, while the mortality of impacted trees are delayed, leading to a gradual decline in LAI. Consequently, an accurate quantification of G_c necessitates consideration of physiological changes within a disturbed ecosystem, rather than relying solely on correlation with mortality.

4.3 | The necessity of adopting an evolution-varied parameter g_1

The parameter g_1 controls the stomatal behaviour (Lin et al., 2015; Medlyn et al., 2011), which is one of the key factors constraining transpiration and carbon fluxes (Bauerle et al., 2014; Tarin et al., 2019). The values of the parameter g_1 differ across plant species due to drastically varied physiological behaviour. The present results further illustrate considerable differences in g_1 depending on regional environmental conditions. In particular, the recommended standard parameterization of the Medlyn model proposed by Medlyn et al. (2011) and De Kauwe et al. (2015), considering global and typical regional scales, and using it for this high-elevation subalpine forest led to a significant overestimation of G_c and T (Figure 5).

Moreover, the values of the parameter g_1 may even temporally change in response to environmental changes (Bauerle et al., 2014) or environmental stress (Section 4.4). The use of evolution-varied parameterization can significantly improve the accuracy in simulations of G_c and T (Figure 6–8). However, current earth system models commonly exclude the possible changes of g_1 under ecosystem disturbance

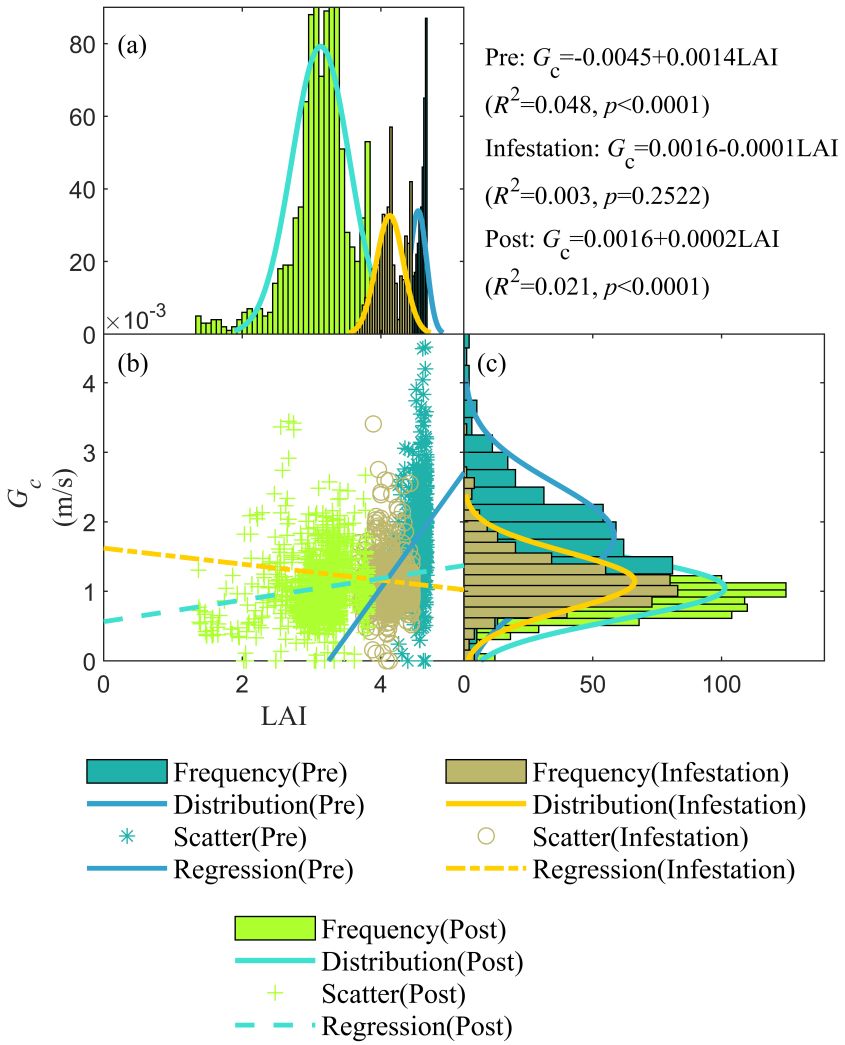

FIGURE 10 The correlation and distribution of G_c with LAI which integrated from the 30-min data with the largest 30% of net radiation and soil water content.

(e.g., bark beetle infestation, drought, and fire) (Franks et al., 2018; Wolz et al., 2017).

4.4 | WUE trends and correlations with g_1

Many studies suggest that the parameter g_1 is a critical parameter related to the physiology of vegetation, reflecting the carbon cost of water use for vegetation (De Kauwe et al., 2015). For the Ball-Berry model and the Leuning model, the slope parameter g_1 represents a balanced strategy between the water costs and carbon benefits of G_c relative to the photosynthetic activity of leaf (Ball et al., 1987). The Medlyn model is derived closely analogous to the Ball-Berry model based on the theory of optimal stomatal behaviour. This theory postulates that stomata should behave such that the carbon gained through photosynthesis is maximized for a given amount of water transpired (Cowan & Farquhar, 1977), which means the parameter $g_{1,M}$ is negatively correlated with WUE (Medlyn et al., 2011). Therefore, the changes in g_1 identified here during a bark beetle infestation may reveal variations in WUE during different periods.

The calculated WUE, based on measured water and carbon fluxes in each year, is shown as a box plot in Figure 11. The results indicated that the WUE in 2008 had similar values as in the pre-infestation period. A decrease in WUE occurred from 2009 to 2011, with a significantly lower minimum value occurring in 2010, after which the WUE increased again during the recovery process of the vegetation in the post-infestation period.

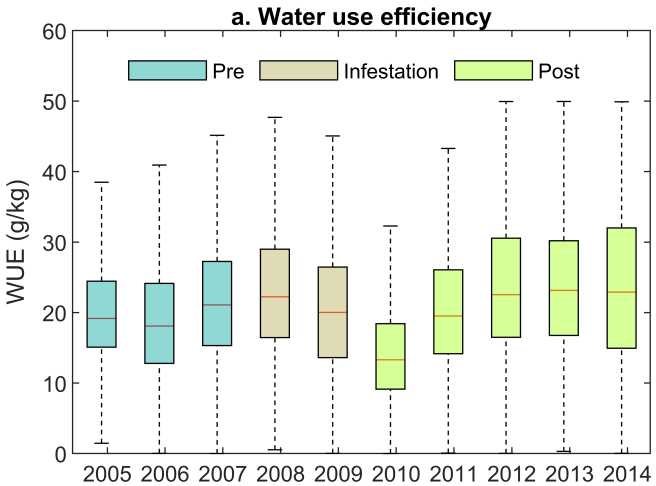

FIGURE 11 Box plots of water use efficiency (WUE) from 2005 to 2014.

During the pre-infestation period (2005 ~ 2007) and post-infestation period (2010 ~ 2014), the decrease of inversely-estimated $g_{1,M}$ was accompanied by an increase in WUE, expressing a negative correlation consistent with the physiology of undamaged and new trees, respectively. In contrast, during the transition between pre-infestation and infestation (2007 ~ 2008), both $g_{1,M}$ and WUE showed increasing trends, indicating a positive correlation between $g_{1,M}$ and WUE.

The positive correlation between g_1 and WUE may be related to the hydraulic failure of infested trees, eventually leading to the death of most of them in 2010 (Frank et al., 2014). Such physiological changes in the infested tree are likely caused by the bark beetle infestation, which hampers the water transport in the xylem, while the photosynthesis may continue (Frank et al., 2014). For infested trees, the transpiration may be smaller than for undamaged trees due to insufficient water transport to opening stomata. But the reduction of stomatal conductance may be smaller than the reduction in transpiration, in order to support sufficient rates of photosynthesis. The reduction of transpiration may be more severe than the reduction in photosynthesis rate, which then causes larger WUE and g_1. When the infested trees die and completely stop extracting water from soil moisture (Frank et al., 2014), the relationship between WUE (calculated by Equation 6) and $g_{1,M}$ can then revert to a negative correlation due to the regrowth of healthy trees in the post infestation period.

5 | CONCLUSIONS

Considering a bark beetle-affected mature spruce forest of the GLEES in Wyoming, USA, we combined flux tower data interpretation using the inverted Penman-Monteith equation with multi-model (the Ball-Berry, Leuning, and Medlyn models) interpretation of canopy-scale stomatal conductance (G_c), showing that:

- The median value of daily T decreased considerably due to the infestation, from 1.14 mm day^{-1} in the pre-infestation period to less than 0.94 mm day^{-1} during infestation.
- LAI decreased by almost half due to the infestation, from 4.55 m^2 m^{-2} in 2007 (pre-infestation) to 2.92 m^2 m^{-2} in 2011 (post-infestation). The G_c and T decreased significantly, mainly at the start of infestation (in 2008). However, the decrease of G_c and T was not as significant as the LAI decrease. This provided evidence of considerable changes in the stomatal behaviour due to the bark beetle infestation.
- In the 5-year post-infection period, T increased again, although did not reach its pre-infestation levels. The LAI recovered only slightly, reaching levels of 3.06 m^2 m^{-2}, and G_c continued to be low, fluctuating between 9.7 × 10^{-4} m s^{-1} to 1.2 × 10^{-3} m s^{-1}.

Taken together, the quantified changes hence provide conclusive results showing that the overall reduction of transpiration was caused not only by the reduced LAI but also by the physiological behaviour of stomatal response. In particular, the positive correlation between g_1 and WUE that was found in response to the onset of infestation, which is likely caused by the bark beetle infestation hampering the water transport in the xylem, while the photosynthesis may continue. This was shown to have important implications for the WUE, which dipped significantly during infestation, after which it recovered as due to regrowth of vegetation in the post-infestation period.

In terms of the capability of the considered state-of-the-art stomatal conductance models to capture and predict the observed ecosystem change dynamics of the GLEES area, we conclude, based on an evaluation of three alternative parametrizations, that:

- The standard parameterization of the stomatal conductance model significantly overestimated G_c and T, showing that it did not reflect the particular environmental conditions in high-elevation subalpine forests.
- Due to the shifting physiological behaviour of stomatal response over time, the model parametrizations that were calibrated and fixed to pre-infestation conditions could not reproduce the actual T dynamics of GLEES area (obtained independently from inverse modelling of flux tower data) equally well as the time variable parametrizations that were re-calibrated to fit the stomatal dynamics in different infestation stages.

More generally, these results imply that the current neglect of the temporal variability of stomatal conductance in ecosystems under stress (including bark beetle infestations) in earth system models may need specific attention to improve the model performance in large-scale water and carbon balances.

ACKNOWLEDGEMENTS

This work was supported by the National Natural Science Foundation of China (Grant No. 41807286), Fundamental Research Project of Science and Technology Department of Qinghai Province (2023-ZJ-705), and by the Czech Science Foundation, GAČR PIF OUT project Grant No. 242-201284.

DATA AVAILABILITY STATEMENT

The data that support the findings of this study are openly available in the GLEES AmeriFlux site at https://doi.org/10.17190/AMF/1246056.

ORCID

Wei Shao https://orcid.org/0000-0003-1478-5892
Ye Su https://orcid.org/0000-0003-3740-7528

REFERENCES

Baca Cabrera, J. C., Hirl, R. T., Schäufele, R., Macdonald, A., & Schnyder, H. (2021). Stomatal conductance limited the CO2 response of grassland in the last century. *BMC Biology*, *19*(1), 50.

Ball, J. T., Woodrow, I. E., & Berry, J. A. (1987). A model predicting stomatal conductance and its contribution to the control of photosynthesis under different environmental conditions. In J. Biggins (Ed.), *Progress in photosynthesis research*: Volume 4 Proceedings of the VIIth

International Congress on Photosynthesis Providence, Rhode Island, USA, August 10–15, 1986 (pp. 221–224). Springer.

Bauerle, W. L., Daniels, A. B., & Barnard, D. M. (2014). Carbon and water flux responses to physiology by environment interactions: A sensitivity analysis of variation in climate on photosynthetic and stomatal parameters. *Climate Dynamics*, *42*(9), 2539–2554.

Bearup, L., Maxwell, R., Clow, D., & McCray, J. (2014). Hydrological effects of forest transpiration loss in bark beetle-impacted watersheds. *Nature Climate Change*, *4*, 481–486.

Beer, C., Ciais, P., Reichstein, M., Baldocchi, D., Law, B. E., Papale, D., Soussana, J. -F., Ammann, C., Buchmann, N., Frank, D., Gianelle, D., Janssens, I. A., Knohl, A., Köstner, B., Moors, E., Roupsard, O., Verbeeck, H., Vesala, T., Williams, C. A., & Wohlfahrt, G. (2009). Temporal and among-site variability of inherent water use efficiency at the ecosystem level. *Global Biogeochemical Cycles*, *23*(2), GB2018.

Buckley, T. N., & Mott, K. A. (2013). Modelling stomatal conductance in response to environmental factors. *Plant, Cell & Environment*, *36*(9), 1691–1699.

Bär, A., Michaletz, S. T., & Mayr, S. (2019). Fire effects on tree physiology. *New Phytologist*, *223*(4), 1728–1741.

Campbell, G. S. (1998). *An introduction to environmental biophysics*. Heidelberg Science Library. Springer. XV,159 pp.

Carlson, A. R., Sibold, J. S., & Negrón, J. F. (2020). Canopy structure and below-canopy temperatures interact to shape seedling response to disturbance in a Rocky Mountain subalpine forest. *Forest Ecology and Management*, *472*, 118234.

Chen, F., Zhang, G., Barlage, M., Zhang, Y., Hicke, J. A., Meddens, A., Zhou, G., Massman, W. J., & Frank, J. (2015). An observational and modeling study of impacts of bark beetle?Caused tree mortality on surface energy and hydrological cycles. *Journal of Hydrometeorology*, *16*(2), 744–761.

Cowan, I. R., & Farquhar, G. D. (1977). Stomatal function in relation to leaf metabolism and environment. *Symposia of the Society for Experimental Biology*, *31*, 471–505.

Damour, G., Simonneau, T., Cochard, H., & Urban, L. (2010). An overview of models of stomatal conductance at the leaf level. *Plant, Cell & Environment*, *33*(9), 1419–1438.

Davis, T. S., Rhoades, P. R., Mann, A. J., & Griswold, T. (2020). Bark beetle outbreak enhances biodiversity and foraging habitat of native bees in alpine landscapes of the southern Rocky Mountains. *Scientific Reports*, *10*(1), 16400.

De Kauwe, M. G., et al. (2015). A test of an optimal stomatal conductance scheme within the CABLE land surface model. *Geoscientific Model Development*, *8*(2), 431–452.

Farquhar, G. D., von Caemmerer, S., & Berry, J. A. (1980). A biochemical model of photosynthetic CO_2 assimilation in leaves of C_3 species. *Planta*, *149*(1), 78–90.

Forzieri, G., Miralles, D. G., Ciais, P., Alkama, R., Ryu, Y., Duveiller, G., Zhang, K., Robertson, E., Kautz, M., Martens, B., Jiang, C., Arneth, A., Georgievski, G., Li, W., Ceccherini, G., Anthoni, P., Lawrence, P., Wiltshire, A., Pongratz, J., … Cescatti, A. (2020). Increased control of vegetation on global terrestrial energy fluxes. *Nature Climate Change*, *10*(4), 356–362.

Frank, J. M., Massman, W. J., Ewers, B. E., & Williams, D. G. (2019). Bayesian analyses of 17 winters of water vapor fluxes show bark beetles reduce sublimation. *Water Resources Research*, *55*(2), 1598–1623.

Frank, J. M., Massman, W. J., Ewers, B. E., Huckaby, L. S., & Negrón, J. F. (2014). Ecosystem CO_2/H_2O fluxes are explained by hydraulically limited gas exchange during tree mortality from spruce bark beetles. *Journal of Geophysical Research: Biogeosciences*, *119*(6), 1195–1215.

Franks, P. J., Bonan, G. B., Berry, J. A., Lombardozzi, D. L., Holbrook, N. M., Herold, N., & Oleson, K. W. (2018). Comparing optimal and empirical stomatal conductance models for application in earth system models. *Global Change Biology*, *24*(12), 5708–5723.

Gash, J. H. C. (1986). A note on estimating the effect of a limited fetch on micrometeorological evaporation measurements. *Boundary-Layer Meteorology*, *35*, 409–413.

Goodsman, D. W., Grosklos, G., Aukema, B. H., Whitehouse, C., Bleiker, K. P., McDowell, N. G., Middleton, R. S., & Xu, C. (2018). The effect of warmer winters on the demography of an outbreak insect is hidden by intraspecific competition. *Global Change Biology*, *24*(8), 3620–3628.

Gu, L., Massman, W. J., Leuning, R., Pallardy, S. G., Meyers, T., Hanson, P. J., Riggs, J. S., Hosman, K. P., & Yang, B. (2012). The fundamental equation of eddy covariance and its application in flux measurements. *Agricultural and Forest Meteorology*, *152*, 135–148.

Henry, C., John, G. P., Pan, R., Bartlett, M. K., Fletcher, L. R., Scoffoni, C., & Sack, L. (2019). A stomatal safety-efficiency trade-off constrains responses to leaf dehydration. *Nature Communications*, *10*(1), 3398.

Hofstetter, R. W., Klepzig, K. D., & Villari, C. (2022). 10 - effects of rising temperatures on ectosymbiotic communities associated with bark and ambrosia beetles. In K. J. K. Gandhi & R. W. Hofstetter (Eds.), *Bark beetle management, ecology, and climate change* (pp. 303–341). Academic Press.

Hubbard, R. M., Ryan, M. G., Stiller, V., & Sperry, J. S. (2001). Stomatal conductance and photosynthesis vary linearly with plant hydraulic conductance in ponderosa pine. *Plant, Cell & Environment*, *24*(1), 113–121.

Jarvis, P. G., Monteith, J. L., & Weatherley, P. E. (1976). The interpretation of the variations in leaf water potential and stomatal conductance found in canopies in the field. *Philosophical Transactions of the Royal Society of London. B, Biological Sciences*, *273*(927), 593–610.

Knauer, J., Zaehle, S., de Kauwe, M. G., Bahar, N. H. A., Evans, J. R., Medlyn, B. E., Reichstein, M., & Werner, C. (2019). Effects of mesophyll conductance on vegetation responses to elevated CO2 concentrations in a land surface model. *Global Change Biology*, *25*(5), 1820–1838.

Lamour, J., Davidson, K. J., Ely, K. S., le Moguédec, G., Leakey, A. D. B., Li, Q., Serbin, S. P., & Rogers, A. (2022). An improved representation of the relationship between photosynthesis and stomatal conductance leads to more stable estimation of conductance parameters and improves the goodness-of-fit across diverse data sets. *Global Change Biology*, *28*(11), 3537–3556.

Leuning, R. (1995). A critical appraisal of a combined stomatal-photosynthesis model for C3 plants. *Plant, Cell & Environment*, *18*(4), 339–355.

Liang, X., Wang, D., Ye, Q., Zhang, J., Liu, M., Liu, H., Yu, K., Wang, Y., Hou, E., Zhong, B., Xu, L., Lv, T., Peng, S., Lu, H., Sicard, P., Anav, A., & Ellsworth, D. S. (2023). Stomatal responses of terrestrial plants to global change. *Nature Communications*, *14*(1), 2188.

Lin, C., Gentine, P., Huang, Y., Guan, K., Kimm, H., & Zhou, S. (2018). Diel ecosystem conductance response to vapor pressure deficit is suboptimal and independent of soil moisture. *Agricultural and Forest Meteorology*, *250-251*, 24–34.

Lin, Y.-S., Medlyn, B. E., Duursma, R. A., Prentice, I. C., Wang, H., Baig, S., Eamus, D., de Dios, V. R., Mitchell, P., Ellsworth, D. S., de Beeck, M. O., Wallin, G., Uddling, J., Tarvainen, L., Linderson, M. L., Cernusak, L. A., Nippert, J. B., Ocheltree, T. W., Tissue, D. T., … Wingate, L. (2015). Optimal stomatal behaviour around the world. *Nature Climate Change*, *5*(5), 459–464.

Lloyd, J., & Farquhar, G. D. (1994). 13C discrimination during CO2 assimilation by the terrestrial biosphere. *Oecologia*, *99*(3), 201–215.

Massman, W. J., & Lee, X. (2002). Eddy covariance flux corrections and uncertainties in long-term studies of carbon and energy exchanges. *Agricultural and Forest Meteorology*, *113*(1), 121–144.

Medlyn, B. E., et al. (2011). Reconciling the optimal and empirical approaches to modelling stomatal conductance. *Global Change Biology*, *17*(6), 2134–2144.

Miner, G. L., Bauerle, W. L., & Baldocchi, D. D. (2017). Estimating the sensitivity of stomatal conductance to photosynthesis: A review. *Plant Cell & Environment*, *40*(7), 1214–1238.

Monteith, J. L. (1965). Evaporation and environment. *Symposia of the Society for Experimental Biology*, *19*, 205–234.

Musselman, R. C. (1994). The Glacier Lakes Ecosystem Experiments Site, Department of Agriculture, Forest Service, Rocky Mountain Forest and Range Experiment Station, Gen. Tech. Rep. RM-249. Fort Collins.

Oleson, K., Lawrence, D., & Bonan, G. B. (2013). Technical description of version 4.5 of the Community Land Model. (CLM) (No. NCAR/TN-503+STR).

Pastorello, G., Trotta, C., Canfora, E., Chu, H., Christianson, D., Cheah, Y. W., Poindexter, C., Chen, J., Elbashandy, A., Humphrey, M., Isaac, P., Polidori, D., Reichstein, M., Ribeca, A., van Ingen, C., Vuichard, N., Zhang, L., Amiro, B., Ammann, C., … Papale, D. (2020). The FLUXNET2015 dataset and the ONEFlux processing pipeline for eddy covariance data. *Scientific Data*, *7*(1), 225.

Pearcy, R. W., Schulze, E., & Zimmermann, R. (2000). Measurement of transpiration and leaf conductance. In *Plant Physiological Ecology*. Springer.

Penman, H. L. (1963). Vegetation and hydrology. *Soil Science*, *96*(5), 357.

Reed, D. E., Ewers, B. E., Pendall, E., Frank, J., & Kelly, R. (2018). Bark beetle-induced tree mortality alters stand energy budgets due to water budget changes. *Theoretical and Applied Climatology*, *131*(1–2), 153–165.

Reichstein, M., Falge, E., Baldocchi, D., Papale, D., Aubinet, M., Berbigier, P., Bernhofer, C., Buchmann, N., Gilmanov, T., Granier, A., Grünwald, T., Havránková, K., Ilvesniemi, H., Janous, D., Knohl, A., Laurila, T., Lohila, A., Loustau, D., Matteucci, G., … Valentini, R. (2005). On the separation of net ecosystem exchange into assimilation and ecosystem respiration: Review and improved algorithm. *Global Change Biology*, *11*(9), 1424–1439.

Ren, J., Adam, J. C., Hicke, J. A., Hanan, E. J., Tague, C. L., Liu, M., Kolden, C. A., & Abatzoglou, J. T. (2021). How does water yield respond to mountain pine beetle infestation in a semiarid forest? *Hydrology and Earth System Sciences*, *25*(9), 4681–4699.

Ren, J., Hanan, E. J., Hicke, J. A., Kolden, C. A., Abatzoglou, J. T., Tague, C. (N.) L., Bart, R. R., Kennedy, M. C., Liu, M., & Adam, J. C. (2023). Bark beetle effects on fire regimes depend on underlying fuel modifications in semiarid systems. *Journal of Advances in Modeling Earth Systems*, *15*(1), e2022MS003073.

Schreiner-McGraw, A. P., Ajami, H., Anderson, R. G., & Wang, D. (2022). Integrating partitioned evapotranspiration data into hydrologic models: Vegetation parameterization and uncertainty quantification of simulated plant water use. *Hydrological Processes*, *36*(6), e14580.

Seidl, R., Thom, D., Kautz, M., Martin-Benito, D., Peltoniemi, M., Vacchiano, G., Wild, J., Ascoli, D., Petr, M., Honkaniemi, J., Lexer, M. J., Trotsiuk, V., Mairota, P., Svoboda, M., Fabrika, M., Nagel, T. A., & Reyer, C. P. O. (2017). Forest disturbances under climate change. *Nature Climate Change*, *7*(6), 395–402.

Sellers, P. J., Bounoua, L., Collatz, G. J., Randall, D. A., Dazlich, D. A., Los, S. O., Berry, J. A., Fung, I., Tucker, C. J., Field, C. B., & Jensen, T. G. (1996). Comparison of radiative and physiological effects of doubled atmospheric CO2 on climate. *Science*, *271*(5254), 1402–1406.

Shao, W., Li, M., Su, Y., Gao, H., & Vlček, L. (2023). A modified Jarvis model to improve the expressing of stomatal response in a beech forest. *Hydrological Processes*, *37*(8), e14955.

Speckman, H. N., Frank, J. M., Bradford, J. B., Miles, B. L., Massman, W. J., Parton, W. J., & Ryan, M. G. (2015). Forest ecosystem respiration estimated from eddy covariance and chamber measurements under high turbulence and substantial tree mortality from bark beetles. *Global Change Biology*, *21*(2), 708–721.

Spitters, C. J. T., Toussaint, H. A. J. M., & Goudriaan, J. (1986). Separating the diffuse and direct component of global radiation and its implications for modeling canopy photosynthesis part I. Components of incoming radiation. *Agricultural and Forest Meteorology*, *38*(1), 217–229.

Tarin, T., Nolan, R. H., Medlyn, B. E., Cleverly, J., & Eamus, D. (2019). Water-use efficiency in a semi-arid woodland with high rainfall variability. *Global Change Biol.ogy*, *26*(2), 496–508.

Vystavna, Y., Holko, L., Hejzlar, J., Perşoiu, A., Graham, N. D., Juras, R., Huneau, F., & Gibson, J. (2018). Isotopic response of run-off to forest disturbance in small mountain catchments. *Hydrological Processes*, *32*(24), 3650–3661.

Webb, E. K., Pearman, G. I., & Leuning, R. (1980). Correction of flux measurements for density effects due to heat and water vapour transfer. *Quarterly Journal of the Royal Meteorological Society*, *106*(447), 85–100.

Wehner, C. E., & Stednick, J. D. (2017). Effects of mountain pine beetle-killed forests on source water contributions to streamflow in headwater streams of the Colorado Rocky Mountains. *Frontiers of Earth Science*, *11*(3), 496–504.

Wolz, K. J., Wertin, T. M., Abordo, M., Wang, D., & Leakey, A. D. B. (2017). Diversity in stomatal function is integral to modelling plant carbon and water fluxes. *Nature Ecology & Evolution*, *1*(9), 1292–1298.

Xu, J., Wu, B., Ryu, D., Yan, N., Zhu, W., & Ma, Z. (2021). A canopy conductance model with temporal physiological and environmental factors. *Science of the Total Environment*, *791*, 148283.

Yang, Y., Anderson, M., Gao, F., Hain, C., Noormets, A., Sun, G., Wynne, R., Thomas, V., & Sun, L. (2020). Investigating impacts of drought and disturbance on evapotranspiration over a forested landscape in North Carolina, USA using high spatiotemporal resolution remotely sensed data. *Remote Sensing of Environment*, *238*, 15.

Yu, O., Goudriaan, J., & Wang, T.-D. (2001). Modelling diurnal courses of photosynthesis and transpiration of leaves on the basis of stomatal and non-stomatal responses Including Photoinhibition. *Photosynthetica*, *39*(1), 43–51.

Zheng, H., Liu, X., Liu, C., Dai, X., & Zhu, R. (2009). Assessing contributions to panevaporation trends in Haihe River Basin, China. *Journal of Geophysical Research: Atmospheres*, *114*, D24105.

Zhou, S., Yu, B., Zhang, Y., Huang, Y., & Wang, G. (2016). Partitioning evapotranspiration based on the concept of underlying water use efficiency. *Water Resources Research*, *52*(2), 1160–1175.

SUPPORTING INFORMATION

Additional supporting information can be found online in the Supporting Information section at the end of this article.

How to cite this article: Li, M., Shao, W., Su, Y., Coenders-Gerrits, M., & Jarsjö, J. (2024). Evidence of field-scale shifts in transpiration dynamics following bark beetle infestation: Stomatal conductance responses. *Hydrological Processes*, *38*(5), e15162. https://doi.org/10.1002/hyp.15162

APPENDIX A

A.1 | CONTRIBUTION ASSESSMENT

Mathematically, for the function $y = f(x_1, x_2, \ldots, x_n)$, the variation of the dependent variable y can be expressed by a differential equation as

$$dy = \sum \frac{\partial f}{\partial x_i} dx_i = \sum f_i' dx_i \quad (A1)$$

where x_i is the i^{th} independent variable and $f_i' = \partial f / \partial x$. Moreover, as y varies with time t, we can rewrite Equation (1) as

$$\frac{dy}{dt} = \sum \frac{\partial f}{\partial x_i} \frac{dx_i}{dt} = \sum f_i \frac{dx_i}{dt} \tag{A2}$$

If we let $TR_y = dx_i/dt$, be the long-term trend in y and x_i, then equation (A2) can be rewritten as

$$TR_y = \sum f_i' TR_i = \sum C(x_i) \tag{A3}$$

If TR_y and TR_i are estimated as the slope of the linear regression for y and x_i against time t given in, C (x_i) can then be estimated as the contribution of x_i to the long-term trend in y, which is exactly the product of the partial derivative and long-term trend in x_i. Therefore, following the equation for reference transpiration estimation.

$$\frac{dT}{dt} = \frac{\partial T}{\partial R_n} \frac{dR_n}{dt} + \frac{\partial T}{\partial T_a} \frac{dT_a}{dt} + \frac{\partial T}{\partial U} \frac{dU}{dt} + \frac{\partial T}{\partial e_a} \frac{de_a}{dt} + \frac{\partial T}{\partial g_s} \frac{dg_s}{dt} + \partial \tag{A4}$$

While δ representing the systemic error in the estimation of the contributions using equation (A4).

Similarly, the variation on canopy conductance G_c can be estimated as:

$$\frac{dG_c}{dt} = \frac{\partial G_c}{\partial LAI} \frac{dLAI}{dt} + \frac{\partial G_c}{\partial g_1} \frac{dg_1}{dt} + \delta, \tag{A5}$$